DEVELOPING AN IONOSPHERIC MAP FOR SOUTH AFRICA

A thesis submitted in partial fulfilment of the requirements for the degree of

MASTER OF SCIENCE

of

RHODES UNIVERSITY

by

DANIEL IZUIKEDINACHI OKOH

June 2009

Abstract

This thesis describes the development of an ionospheric map for the South African region using the current available resources. The International Reference Ionosphere (IRI) model, the South African Bottomside Ionospheric Model (SABIM), and measurements from ionosondes in the South African Ionosonde Network, were incorporated into the map. An accurate ionospheric map depicting the f_oF_2 and h_mF_2 parameters as well as electron density profiles at any location within South Africa is a useful tool for, amongst others, High Frequency (HF) communicators and space weather centers. A major product of the work is software, written in MATLAB, which produces spatial and temporal representations of the South African ionosphere. The map was validated and demonstrated for practical application, since a significant aim of the project was to make the map as applicable as possible. It is hoped that the map will find immense application in HF radio communication industries, research industries, aviation industries, and other industries that make use of Earth-Space systems. A potential user of the map is GrinTek Ewation (GEW) who is currently evaluating it for their purposes.

Acknowledgements

I would like to express my gratitude to my supervisors, Dr. Lee-Anne McKinnell and Dr. Pierre Cilliers, for their excellent support and contribution.

Special thanks to the National Astrophysics and Space Science Programme (NASSP) and the Hermanus Magnetic Observatory (HMO) for their financial support, and for the opportunity to use their facilities. I am immensely grateful for the overwhelming number of opportunities I had during the course of this research.

I appreciate

- Dr. Dieter Bilitza of the International Reference Ionosphere (IRI) for making the IRI model available;
- Dr. Lee-Anne McKinnell for providing the South African Bottomside Ionospheric Model (SABIM) and the ionosonde data;
- Dr. Ben Opperman, Mr. Patrick Sibanda, Mr. John Bosco Habarulema and Mr. Stefan Lotz for helping with the GPS data and with programming techniques;
- Mrs Jeanne Cilliers for carefully proof-reading this thesis;
- Prof. Norman Ratcliffe and Prof. Paul Cannon for their ray-tracing software.

I heartily appreciate my colleagues at the HMO for their company, invaluable support, and for providing me with a home away from home. Many thanks to the HMO staff members for their care and warm disposition.

My heartfelt gratitude goes to my family members and friends who have invested their energy, time and resources in me. Special thanks to my parents, Mr. and Mrs. Godwin Okoh, for all their tireless efforts.

Lastly and most importantly, I thank the Almighty God for His grace upon my life. He has being my comfort, my strength, and my guide. He surely has kept me, even though I am not worthy of His mercies.

Contents

List of Figures

List of Tables

Chapter 1

Introduction

1.1 Introduction to the Project

The aim of this project is to develop a map of the ionosphere over the South African region based on available data sources. The map is essentially a computer programme that graphically represents the distribution of ionospheric electrons over the region, in time and in space. The purpose of the project is fully discussed in section 1.4. The available sources of data (ionospheric models and ionosondes) are discussed in chapter 2, and the way in which they have been combined to develop the map, is discussed in chapter 3.

The ionosphere affects our lives in diverse ways, ranging from its usefulness in High Frequency (HF) radio propagation, to its attenuation of radio signals that have to pass through it. By extending our knowledge to lesser known areas of the ionosphere, use of the ionosphere can be greatly enhanced, and significant allowance can be made for the effects ionospheric behaviour can have on signals passing through these altitudes.

1.2 A General Overview of the Ionosphere

1.2.1 The Ionosphere

The ionosphere is the region of our atmosphere extending from a height of about 50 km to about 1000 km. What distinguishes the ionospheric region from other regions of the atmosphere is that it contains significantly more charged particles. Kohl et al. (1996, p. 181) explained that the main source of plasma and energy for the ionosphere is solar extreme ultraviolet (EUV) and ultraviolet (UV) radiation, but that magnetospheric electric fields and

particle precipitation have significant effects on the system. Ratcliffe (1972, pp. 3-36) and Kohl et al. (1996, pp. 181-185) have detailed descriptions of processes at work within the ionosphere.

1.2.2 Regions of the Ionosphere

Based on chemical composition, level of ionisation, and variability, the ionosphere is sub-divided into the following regions.

***D* Region:**

The *D* region is the lowest region of the ionosphere lying at approximately 50 km to 90 km above the earth's surface. The intensity of solar radiation reaching these altitudes is so small that relatively weak ionizations, and hence relatively low electron densities, are found in the region. The *D* region corresponds to a sparse layer of polyatomic ion clusters with densities in the range 10^2 to 10^4 cm^{-3} (Giraud & Petit 1978, p. 22). At night, the ionization in this layer almost, but not completely, disappears. The layer reduces greatly after sunset, but remains due to the ionization effect of galactic cosmic rays (Bonnet & Woltjer 2008, p. 360). Radio waves cannot be reflected from the *D* layer but pass through to the strongly reflecting *E* and *F* regions. Bonnet and Woltjer (2008, p. 360) explain that the *D* layer is mainly responsible for absorption of HF radio waves, particularly at 10 MHz and below, with progressively smaller absorptions as the frequency gets higher.

***E* Region:**

The *E* region is the region immediately above the *D* region, and extends from altitudes of about 90 km to 120 km. As expected, the ionization in this region is stronger than that in the *D* region, and is strongly diminished at night. The *E* region corresponds to a moderately dense (10^3 to 10^5 cm^{-3}) layer of molecular ions NO^+ and O_2^+ in the midst of which fluctuate thin layers of atomic ions occasionally peaking in the so-called 'sporadic *E*' (E_s) phenomenon (Giraud & Petit 1978, p. 22). Bonnet & Woltjer (2008, p. 360) noted that charged particles in the *E* layer are due to the ionization of molecular oxygen (O_2) by soft X-rays and EUV radiations (1-10 nm), and that the layer is able to reflect radio waves with frequencies less than about 10 MHz. They also pointed out that, at night, the *E* layer begins to disappear because the primary source of ionization (the sun) is no longer present.

***F* Region:**

The *F* region is immediately above the *E* region, and extends to well above 300 km. This region contains the greatest density of free electrons, making it the most important for long distance radio propagation. The *F* region corresponds to a dense layer (10^5 to 10^6 cm^{-3}) of atomic O^+ ions (Giraud & Petit 1978, p. 22). Ionization here is mainly due to photo-ionization of atomic oxygen by extreme ultraviolet solar radiation. At night, the *F* region is mainly one layer, but during daylight hours it is divided into two sub-layers, the F_1 and F_2 layers. The F_2 layer is the higher layer of the two, and contains larger electron densities than the F_1 layer. A greater concentration of free electrons and ions is found in the F_2 region than anywhere else in the atmosphere. Giraud & Petit (1978, p. 22) also pointed out that the F_1 region is the transition between molecular and atomic ions, while the F_2 region is the peak of O^+ ions. More details on the *F* region dynamics can be found in Ratcliffe (1972, pp. 55-57).

1.2.3 Experimental Investigation of the Ionosphere

A good number of instruments are today being used to probe the ionosphere. For this project, data from the 4 South African ionosonde stations located at Grahamstown (33.3°S, 26.5°E), Madimbo (22.4°S, 30.9°E), Louisvale (28.5°S, 21.2°E), and Hermanus (34.2°S, 19.2°E) were used. Ionosondes are HF radars that send radio wave pulses straight up at vertical incidence into the ionosphere, and receive the reflected pulses. By measuring the time of flight of the transmitted pulse, the instrument is able to provide a wealth of information about the ionosphere. The ionosondes used in this work are discussed in more detail in Chapter 2. Kohl et al. (1996, pp. 440-458) and Davies (1990, pp. 89-110) contain detailed and general information on the principle of operation of ionosondes.

Besides using ionosondes, other ways that the ionosphere may be studied include the use of incoherent scatter radars, and experiments on board rockets and balloons. Since data from these instruments were not directly used in this project and are therefore not covered in detail within this thesis, the reader is referred to Davies (1990, pp. 106-112) for more detail.

1.3 High Frequency Radio Propagation through the Ionosphere

High Frequency radio waves are radio waves having frequencies in the range of between 3 MHz and 30 MHz. The bottomside ionosphere (the region of the ionosphere lying between about 80 km and 350 km) contains sufficient density of charged particles to cause substantial refraction and reflection of these waves as they attempt to pass through it.

1.3.1 The Ionosphere as an HF Radio Reflector

An important aspect of the ionosphere is its ability to reflect HF radio waves that would have left the Earth, making it possible to reach several other places on Earth, where the signals would not have reached otherwise. Consider, for instance, an HF radio signal transmitted from point A as shown in figure 1-1.

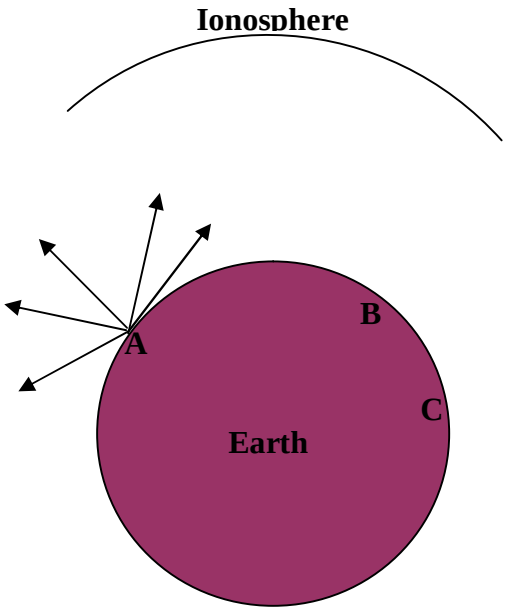

Figure 1-1: A diagram to illustrate that an HF radio signal transmitted from one point on Earth cannot directly reach several other points on it

The radio signal leaves in all directions, but since radio waves travel in straight lines, they can't get to places like B and C. The ionosphere, here, can play the role of a reflector; the ionosphere can reflect these waves allowing the signals to reach places like B and C, as illustrated in figure 1-2.

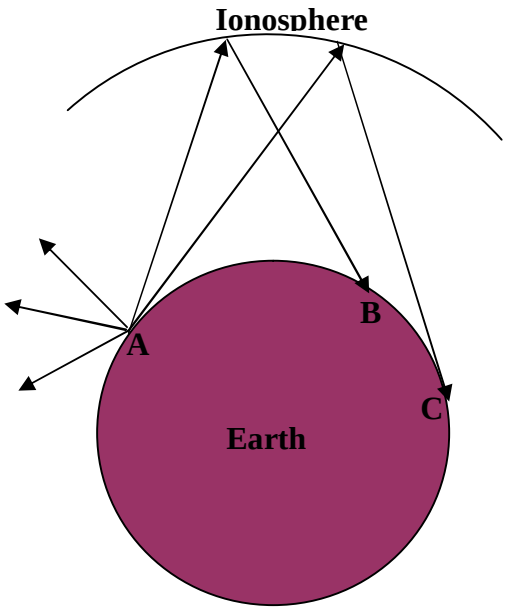

Figure 1-2: A diagram to illustrate that the ionosphere reflects HF radio signals allowing them to reach other places on Earth

The path of such radio waves is defined by the distribution of electrons in the ionosphere, and by the frequencies of the transmitted radio waves. The ray-tracing idea is needed to precisely predict the path of such radio waves, and is discussed in section 1.3.4.

1.3.2 Plasma Oscillations in the Ionosphere

Plasma electrons in the ionosphere oscillate with a characteristic frequency known as the plasma frequency. Lorentz (1916, p.133) explained that when electromagnetic waves pass through an ionized medium, they set electrons into vibration. Chen (1984, p. 82) further discussed the phenomenon by explaining that when electrons in plasma are slightly displaced from background ions, a Coulomb force is generated in such a direction as to drag the electrons back to their original positions, but that due to their inertia, these electrons overshoot the intended position and are trapped in an oscillation about that position. This is called plasma oscillation and the characteristic frequency of the oscillation is known as the plasma frequency.

Chen (1984, pp. 83-85) also showed that the plasma frequency (in units of radians per second) at any point in a plasma is given by

$$\omega_p = 2\pi f = \sqrt{\frac{ne^2}{\varepsilon_0 m}} \quad (1\text{-}1)$$

where f is the corresponding Plasma frequency (in Hertz), n is the number density of the electrons (in electrons per cubic meter), $e = 1.60 \times 10^{-19}$ C is the electron charge, $\varepsilon_0 = 8.85 \times 10^{-12}$ Fm^{-1} is the dielectric constant, and $m = 9.11 \times 10^{-31}$ kg is the electron mass. Since all other quantities on the right hand side of equation (1-1), except the electron density (n) are constants, these quantities can be substituted for their values, and the frequency can be put into units of MHz, transforming equation (1-1) to the simpler form of equation (1-2) with the electron density still in electrons per cubic meter.

$$n = 1.24 \times 10^{10} f^2 \quad (1\text{-}2)$$

Equation (1-2) shows a square-law relation between the plasma frequency, f, and the electron density, n.

Physically, the plasma frequency represents the highest radio frequency that a portion of the ionosphere is able to reflect if radio waves are at normal incidence to the ionosphere. In general, a radio signal will penetrate or traverse a portion of the ionosphere if the radio frequency is greater than the plasma frequency. If the radio frequency is less than or equal to the plasma frequency, the signal is reflected by the ionosphere.

1.3.3 Definition of Some Ionospheric Parameters and Symbols

Each one of the bottomside ionospheric layers has a local peak concentration of electrons in that layer. This is referred to as N_mF_2 for the F_2 layer, N_mF_1 for the F_1 layer, and N_mE for the E layer. The corresponding heights where these peaks occur are referred to as h_mF_2 for the F_2 layer, h_mF_1 for the F_1 layer, and h_mE for the E layer.

Equations (1-1) and (1-2) above imply that the plasma frequencies are greater in parts of the ionosphere where the electron densities are greater. Points of peak electron densities are, therefore, points of peak plasma frequencies. The peak plasma frequencies are also called the critical plasma frequencies, and are denoted f_oE, f_oF_1, and f_oF_2 for the E, F_1, and F_2 layers respectively.

Since the F_2 layer will always contain the highest density of electrons in the ionosphere, the f_oF_2 value is the highest plasma frequency obtainable in the ionosphere, and it represents the highest possible radio frequency that the ionosphere can reflect at normal incidence of the radio waves. It follows, from equation (1-2), that the f_oF_2 and N_mF_2 are connected by the equation

$$N_mF_2=1.24\text{x}10^{10}(f_oF_2)^2 \qquad (1\text{-}3)$$

1.3.4 Ray Tracing through the Ionosphere

Ray tracing is a way of determining the path of radio waves through a system with regions of varying propagation properties. HF radio communicators use ray tracing to precisely determine the paths of HF radio waves as they propagate through the ionosphere. The process basically involves a step-by-step integration of differential equations that describe the propagation of these waves through dispersive and anisotropic media like the ionosphere. Unlike optical ray tracing, in which the refractive index is typically constant for a given medium, ray tracing through the ionosphere must account for the complexities of a spatially and temporally varying refractive index, where changes in the ionospheric electron density correspond to changes in the refractive index. Haselgrove (1955) described a method of using Hamilton's equations for geometrical optics to calculate the path of rays through the ionosphere. The method offers a high speed of computation, puts no restriction on having a stratified ionosphere nor a constant magnetic field over the Earth, and takes into account the curvature of the Earth.

Figure 1-3 below is an illustration of ray tracing through the ionosphere using an analytic, path-segmented, and quasi-parabolic ray-tracing approach (Norman & Cannon 1997; 1999). This approach was used to illustrate the application of the project in chapter 4.

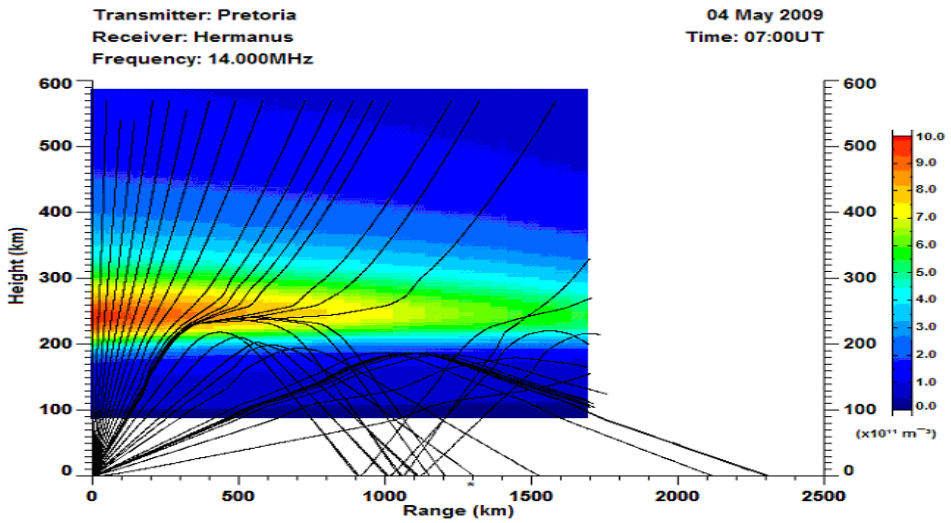

Figure 1-3: An illustration of ray tracing through the ionosphere

1.4 Purpose of the Project

The project is aimed at developing a map of the ionosphere over South Africa using the best possible combination of sources available. The available sources are the International Reference Ionosphere (IRI) model, the South African Bottomside Ionospheric Model (SABIM) and scaled measurements from the 4 ionosondes in the South African ionosonde network. These sources were combined in such a way as to develop a map of the behaviour of South Africa's ionosphere that is as accurate as possible. Chapter 2 is a detailed discussion of these sources, while the development of the map is discussed in chapter 3.

An ionospheric map is essentially a computer programme that shows spatial and temporal representations of ionospheric parameters like the electron density, critical plasma frequencies, etc., for every geographical location on the map. Such a programme will rely on ionospheric models and on measurements taken by ionospheric instruments for the values of the parameters at each location. The main goal of an ionospheric model is to provide a mathematical description of the ionosphere as a function of position in space, and time (considering the fact that ionospheric behaviour changes with time, location, season, magnetic and solar activity).

The drive behind this project is based on a requirement by the communications, defence, aviation, and research industries. Communications and Defense Industries need ionospheric maps for direction finding and propagation predictions of HF radio waves. Aviation

industries need them to correct for ionospheric effects on their positioning and navigation systems. A potential user of the map is Grintek Ewation. Grintek Ewation is a systems engineering company which produces products and systems, and provides services to government institutions and national defense forces. Grintek Ewation has been the electronic warfare systems house for the South African National Defense Force (SANDF) for the past 30 years (Grintek Ewation 2009). The map will also be of great value to ionospheric and space weather researchers, and will be made available as a space weather product on the Hermanus Magnetic Observatory space weather website (http://spaceweather.hmo.ac.za/).

1.5 Overview of the Thesis

Chapter 2 of the thesis discusses the models and facilities used in developing the map. It begins with a discussion of the South African Bottomside Ionospheric Model (SABIM), then the International Reference Ionosphere (IRI) model, and concludes with a treatment of the 4 South African ionosonde stations that were used in the work.

Chapter 3 describes the development of the map and results from the map. It starts by discussing the way in which the data sources were incorporated into the map, then the project algorithm, the physical and mathematical techniques that were used, and finally results from the map.

The project validation is done in Chapter 4. It starts with a brief description of resources that were used in the validation process; ray-tracing software, and total electron content (TEC) data derived from global positioning system (GPS) observations within South Africa. It concludes with a description of how these tools were utilized for the validation of the map.

Chapter 5 describes the conclusion of the project. It is a succinct summary of the results, and proposes future work required to further improve on the map.

Chapter 2

Available Data Sources

2.1 The South African Bottomside Ionospheric Model (SABIM)

SABIM is a model of South Africa's bottomside ionosphere developed by Dr Lee-Anne McKinnell, a Space Physics researcher with the Hermanus Magnetic Observatory (HMO), and Rhodes University, South Africa (McKinnell 2008b). SABIM was developed using an archive of data from the 3 South African ionosonde stations located at Grahamstown (33.3°S, 26.5°E), Madimbo (22.4°S, 30.9°E) and Louisvale (28.5°S, 21.2°E). These stations are located as shown in figure 2-1 below.

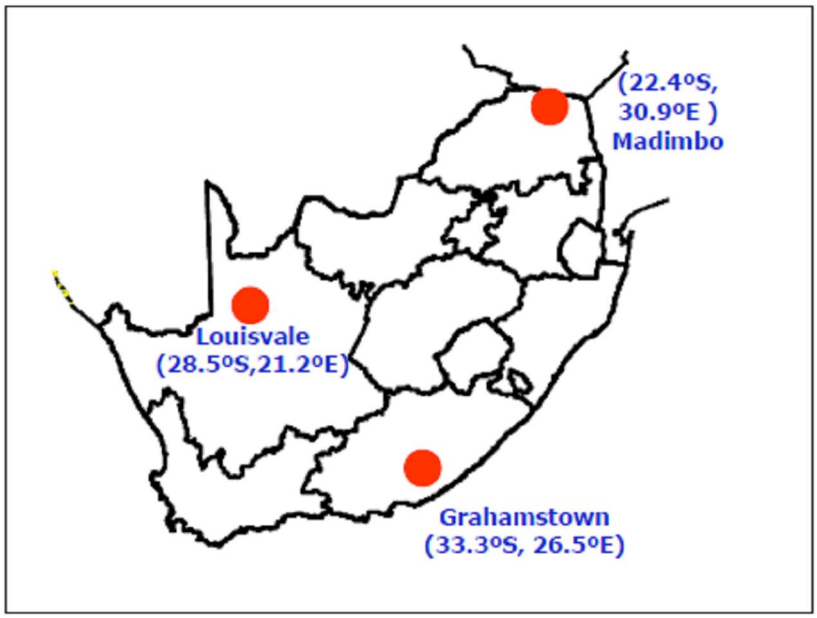

Figure 2-1: Locations of the 3 South African ionosonde stations used to develop SABIM (McKinnell 2008c)

2.1.1 The Development of SABIM

SABIM was developed using the technique of training Neural Networks (NNs) to learn from, and adapt to the pattern of archived data. A NN is simply a computer algorithm that is trained to learn the relationship between an output and a set of given input parameters (McKinnell 2008a). Gurney (1997, p.1) explains that the processing ability of the network is stored in the inter-unit connection strengths, or weights, obtained by a process of adaptation to, or learning from, a set of training patterns. See Gurney (1997, pp. 1-234) for very detailed information on NNs. To develop the model, NNs were trained to predict the parameters (including coefficients of a Chebyshev polynomial) needed to construct an electron density profile for given inputs.

SABIM was previously called the LAM model (McKinnell 2008b). The earliest version of SABIM made use of data from the Grahamstown station only, limiting its applicability spatially to just that geographic location. Version 2 of SABIM was extended to include data from the other 2 stations, and was more representative of the entire South African latitude range (McKinnell 2008b). The latest version of SABIM is version 3, and is the version used in this work. Version 3 of SABIM has now been updated to include all available data to the end of 2006 and is now more representative of geophysical parameters like the solar and magnetic activities. Detailed information about Version 1, Version 2, and Version 3 of SABIM can be found respectively in McKinnell (2002, pp. 1-150), McKinnell (2005), and McKinnell (2008b). Currently, SABIM is being updated every 2 years and is being used for Southern African ionospheric research as well as in direction finding and HF radio communication applications (McKinnell 2008c).

2.1.2 SABIM Inputs and Outputs

The required inputs are the geographical latitude, geographical longitude, year, day number (day of the year), and hour. McKinnell (2008b) explains that instead of the year, the solar and magnetic activity variables may be entered. The model uses the year to calculate the solar and magnetic variables based on provided files containing the daily values of each. “In the latter case, where the solar and magnetic variables are entered, the model will determine a suitable year based on the given solar variable, and determine the magnetic dip angle and declination for that year. When this model is implemented in the field, the source for the inputs will be adjusted to suit the environment within which the model will be run” (McKinnell 2008b).

The output is basically an f(h) profile (that is a measure of the electron densities at various altitudes) corresponding to the given input parameters. Figure 2-2 below is a flow diagram illustrating the process that the model follows in determining the predicted profile. McKinnell (2008b) has more detailed information on the process.

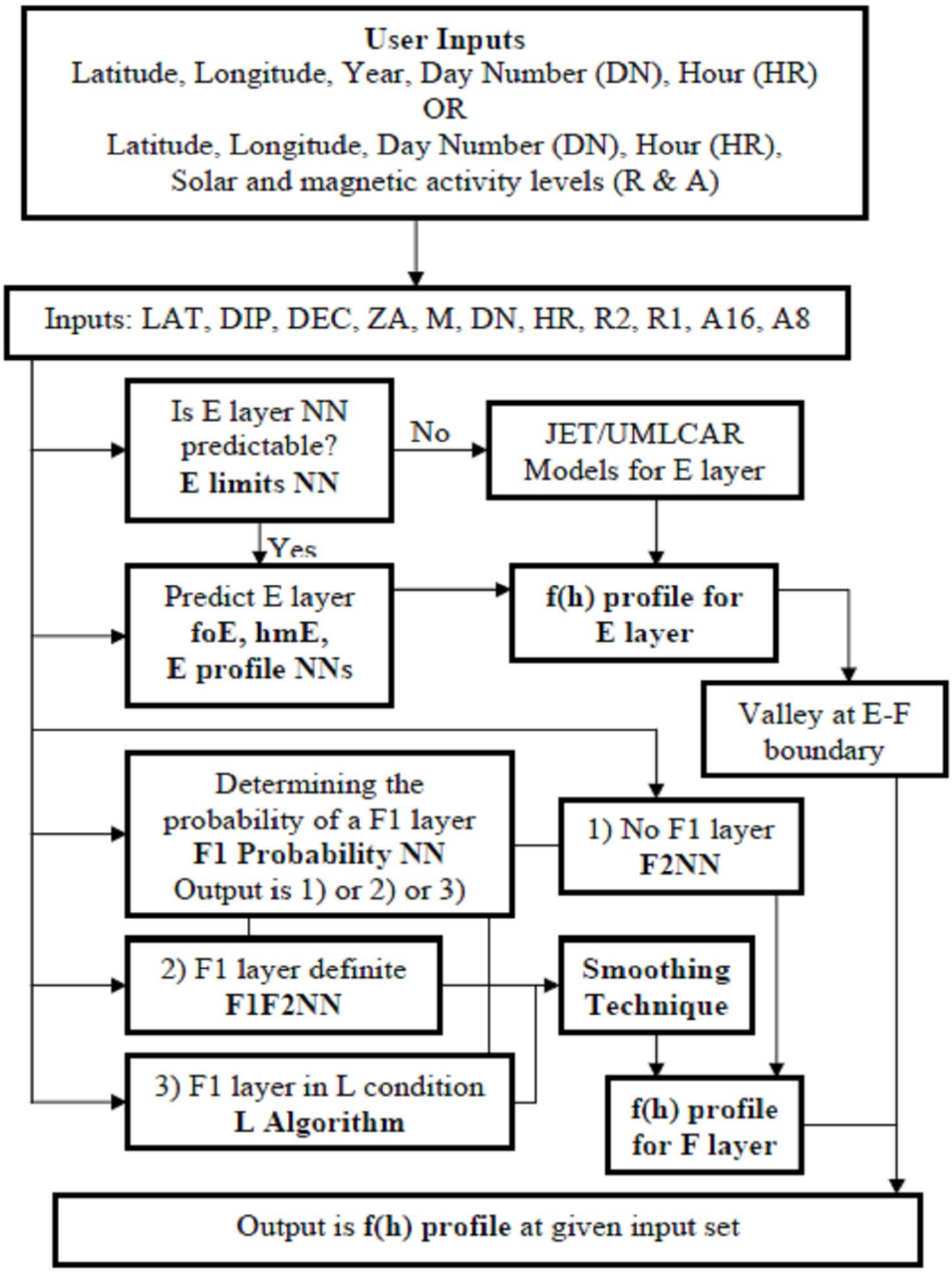

Figure 2-2: A flow diagram illustrating the process followed by SABIM in determining the predicted profile (McKinnell 2008c)

For the purpose of this work, SABIM was implemented as an executable programme produced from a code written in the C programming language. Amongst other parameters, SABIM can provide the peak parameters f_oF_2 and h_mF_2; the f_oF_2 is the peak value on the f(h) profile, representing the maximum electron density, while the h_mF_2 is the corresponding height of the peak.

2.1.3 SABIM Performance and Limitations

SABIM was developed due to the insufficiencies observed in using global ionospheric models for the South African region. McKinnell & Poole (2004) noted that the IRI model is known to be inaccurate in the South African region due to a historical paucity of available data for the region. According to them, comparisons with the IRI global model showed that, for Grahamstown, a NN-based model predicted the noon value of f_oF_2 more realistically than the IRI. Earlier work done by McKinnell (2002, pp. 127-130) showed that SABIM predictions were better than IRI predictions over Grahamstown when compared to measured data from the Grahamstown ionosonde, especially in the F_1 region. A powerful feature of SABIM includes its ability to predict the probability of existence of an F_1 layer and apply corrective measures to ensure a realistic result (McKinnell 2008c).

SABIM limitations are mainly in the amount of available data for training the NNs. According to McKinnell (2008b), the limitations placed on a NN-based model depend solely on the database that was used in the development of the model. She pointed out that since the model incorporated data from just the 3 South African ionosondes, it can, in theory, only be used to predict electron density profiles within the latitude range bounded by the ionosonde stations (that is, between -22.4 to -33.3 degrees) since NNs are known to interpolate well, but not to extrapolate well. McKinnell (2008c) suggests that these limitations will be overcome subsequently by ingesting into the model, recently archived data from the 3 ionosonde stations, and from the Hermanus ionosonde (34.24°S, 19.22°E) installed in July 2008.

2.2 The International Reference Ionosphere (IRI) Model

The International Reference Ionosphere (IRI) is the international standard for the specification of ionospheric densities and temperatures (Bilitza 2001). The IRI is an empirical model developed using available data from all around the world. The model was developed and is being maintained by a working group that is jointly sponsored by the Committee on Space Research (COSPAR) and the International Union of Radio Science (URSI). The aim of the IRI is to establish a summary compendium of height profiles through the ionosphere for the four main plasma parameters, namely plasma density, temperatures of ions and electrons, and ion composition (McNamara & Wilkinson 1983). The model describes monthly averages of ionospheric densities and temperatures (Bilitza & Reinisch 2008).

2.2.1 Development of the IRI Model

The IRI project began in the late sixties, and since then several versions have been released both in hard copy and in computer-readable formats. The first widely circulated edition of the model was IRI-78 (computer programme: Version No. *5).* A detailed account of the history and development of the IRI can be found in Bilitza et al. (1993). The latest version of the IRI model is the IRI-2007, and is the version used in this work. An interesting enhancement to the IRI-2007, which proved useful for this study, is the inclusion of two new options for the topside electron density, namely the corrected IRI topside and the NeQuick topside models. The topside profile is of special importance because of its impact on the total electron content (TEC), which is the prime parameter needed for many ionospheric model applications (Bilitza & Reinisch 2008). The NeQuick topside option was used to obtain TEC values from the IRI for the testing and validation of this work (described in chapter 4). According to Bilitza & Reinisch (2008), the NeQuick model is the most mature of the different proposals for the IRI topside. Several other changes were introduced with this version; Bilitza & Reinisch (2008) give a detailed description. The IRI is updated yearly during special IRI workshops.

2.2.2 IRI Inputs and Outputs

The main IRI-website is available at http://iri.gsfc.nasa.gov. The IRI model is available for use either as a web-based application at http://omniweb.gsfc.nasa.gov/vitmo/iri_vitmo.html, or as a FORTRAN source code at ftp://nssdcftp.gsfc.nasa.gov/models/. For the purpose of this work, the FORTRAN source code was used so as to allow the implementation of user-defined automatic operations.

The input parameters required by the IRI model depend on what output is desired. In this case, the electron density profile is desired, and the required inputs are the geographical latitude, geographical longitude, year, day number (day of the year), hour, and a choice of options to be used in the model. The IRI options used in this work are exactly the standard IRI options (default for the IRI model), except for cases were there was a need to supply the IRI model with given f_oF_2 and h_mF_2 values. See appendix A for a description of the standard IRI options.

2.2.3 Performance and Limitations of the IRI Model

Since its inception in 1969, the IRI model has been steadily improved with newer data and with better mathematical descriptions of global and temporal variation patterns (Bilitza & Reinisch 2008), and has been recommended for international use by COSPAR and URSI. A large number of independent studies have validated the IRI model in comparisons with direct and indirect ionospheric measurements not used in the model development (Bilitza & Reinisch 2008). Examples of such studies can be found in Adewale et al. (2009), Sethi et al. (2009), Soicher et al. (1995), and several others. A comparison with IRI is often one of the first science tasks by an ionospheric, satellite or rocket team (Bilitza & Reinisch 2008).

By using the IRI standard options in this work, the STORM model was switched on; this offers storm-time corrections to the f_oF_2 values, but not to the h_mF_2 values. The STORM option is also only available for requested dates that lie within the IRI Ap index range (that is from 1958 to August 2009).

Although the IRI patterns often agree with observations, substantial differences are also often noticed. A number of studies have noted discrepancies between the IRI model and measurements, especially at high latitudes and during high solar activities (Bilitza & Reinisch

2008). Work done by Chuo & Lee (2008), for instance, shows that at Taiwan, the percentage deviation of the observed f_oF_2 values with respect to the IRI model varies from 5% to 80% during nighttime and 2–17% during daytime. For South Africa, Adewale et al. (2009) showed that the IRI generally overestimated h_mF_2 for both quiet and disturbed days. Certain discrepancies between the IRI and observations were also reported in Sethi et al. (2008), De Medeiros et al. (2003), and Bhuyan & Borah (2007). Bilitza et al. (1993) points out shortcomings and limitations of the IRI, discusses ways of overcoming them, and suggests priorities for a list of work items that the IRI group has to tackle in the future.

2.3 The South African Ionosonde Network

The South African Ionosonde Network (HMO 2009) currently comprises of 4 ionosonde stations located at Grahamstown (Eastern Cape, 33.3°S, 26.5°E), Louisvale (Northern Cape, 28.5°S, 21.2°E), Madimbo (Limpopo, 22.4°S, 30.9°E) and Hermanus (Western Cape, 34.4°S, 19.2°E).

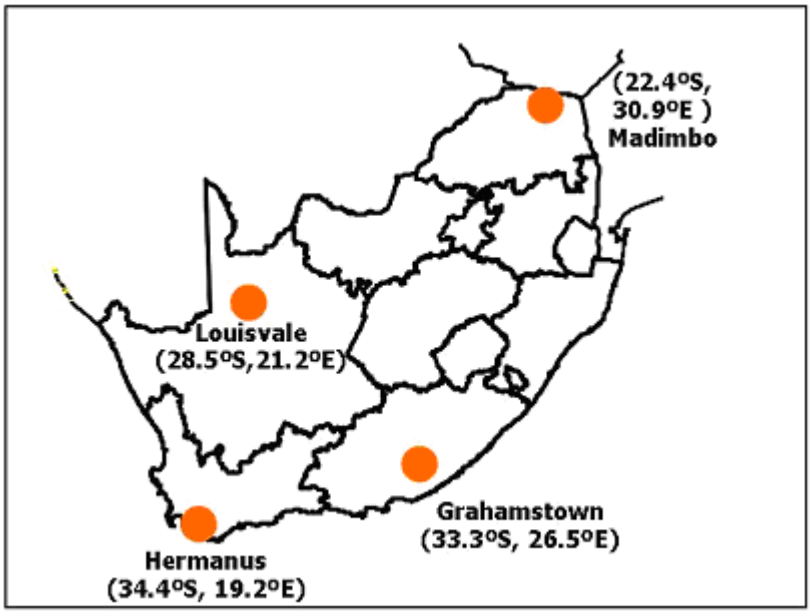

Figure 2-3**:** Locations of the 4 South African ionosonde stations (HMO 2009)

The 4 ionosondes are all digisondes produced by the University of Massachusetts, Lowell Center for Atmospheric Research (UMLCAR). Digisondes are modern digital ionosondes. The three older digisondes (located at Grahamstown, Madimbo and Louisvale) are owned by the South African National Defence Force (SANDF), and are four-receiver Digisonde

Portable Sounder (DPS-4) models. The Digital Portable Sounder (DPS) is capable of providing real-time on-site processing and analysis. It has a transmit antenna and four crossed loop receive antennas. According to UMLCAR, in the DPS the signals from the four crossed loop receive antennas are fed into the antenna switch box, which either selects one signal to feed to the single receiver card or combines all four in phase. They explain that in the DPS-4 (four-channel receiver variant) one receiver is dedicated to each receive antenna.

The digisonde at Grahamstown has been operational since 1996, while those at Madimbo and Louisvale have been operational since 2000. At the Grahamstown station, a Barry Research Chirp sounder operated prior to the installation of the DPS-4 and so there is a database of ionospheric data for Grahamstown going back to 1973 (HMO 2009).

The Hermanus ionosonde is a new model DPS-4D digisonde donated to the Hermanus Magnetic Observatory, South Africa, by the South African Department of Communications.

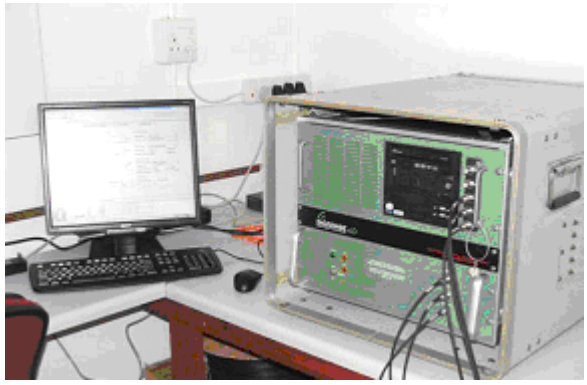

Figure 2-4: The newly installed DPS-4D digisonde at Hermanus (McKinnell 2008d)

The new digisonde has improved capabilities over the previous generation of digisondes. Apart from investigating the vertical profile of the ionosphere, the new digisonde can also perform drift measurements to look at ionospheric tilt, angle of arrival and phase measurements of the incoming signal, doppler velocity, and oblique soundings. Its installation was completed in July 2008.

The Grahamstown and Hermanus ionosondes are set to a 15-minute resolution, while the Louisvale and Madimbo ionosondes are at a 30-minute resolution. For this reason, the temporal resolution of the ionospheric map was set to 30 minutes.

Data was incorporated into the map from the ionosondes in the SAO.XML file format. The SAO.XML file format is one of the file formats for data generated by the ionosondes. Detailed information about the format can be found on http://ulcar.uml.edu/SAOXML/SAO.XML%205.0%20specification%20v1.0.pdf .

The Department of Physics and Electronics at Rhodes University partners the HMO in the South African ionospheric data collection, archiving and distribution (HMO 2009). Other information about these ionosondes can be found on the UMLCAR website for digisondes (http://ulcar.uml.edu/digisonde.html), and on the HMO space weather website (http://spaceweather.hmo.ac.za/).

In conclusion, the IRI is the international standard for the ionosphere, the SABIM is an adaption for the South African region, and the South African ionosonde network provides 'true' ionospheric information for the region. These 3 sources are the only considered sources for constructing a South African ionospheric map, and this is the reason they've been discussed in this chapter. The next chapter discusses how these sources were put together to develop the ionospheric map.

Chapter 3

Developing the Ionospheric Map

A major product of this project is software (written in the MATLAB programming language) that generates maps illustrating spatial and temporal representations of the South African ionosphere. The software produces maps of the f_oF_2 values, and electron density profiles of the ionosphere above specific locations in the South African region for a given set of input parameters.

3.1 Combining the Data Sources

The data sources considered for the development of the map are the IRI model, SABIM, and measured data from the 4 South African ionosonde stations. In this section, the way in which these sources were combined to develop the map is discussed.

3.1.1 Combining SABIM and the IRI Model

To produce the map of f_oF_2 values, SABIM was used inside the triangular region bounded by the 3 ionosonde stations that were used in the development of the model, and the IRI model was used outside that region. A smoothing function was introduced at the boundary of the regions, so that SABIM still contributes outside the triangular region, but that this contribution decreases as the distance to the closest edge of the triangle increases. This smoothing function is discussed in section 3.4.1.

The rationale behind this combination is that SABIM has been shown to perform more accurately than the IRI model inside of the triangular region bounded by the 3 ionosonde stations that were used to develop the model (Poole & McKinnell 2000), but that its

performance outside of that region is not guaranteed. According to McKinnell (2008b), NNs (the technique used in the development of SABIM) are known to interpolate well but they do not extrapolate well.

3.1.2 Incorporating the Ionosonde Data

Ionosonde measurements provide the most accurate recordings of ionospheric behaviour, so in the development of the map this data source receives first priority. Measurements from the ionosondes were further used to adapt the produced f_oF_2 map to the ionosonde measurements. For each ionosonde location, the programme calculates the difference between the ionosonde's f_oF_2 measurement and the f_oF_2 value calculated by the existing modeled map at the ionosonde location. It then fits a best plane (discussed in section 3.4.2) of these differences over the whole map. The programme uses this plane to adjust the f_oF_2 map to measurements from the ionosondes.

3.1.3 Generating the Electron Density Profiles

To generate the electron density profile for any location within the map, the programme uses the IRI model, but supplies it with the location's f_oF_2 and h_mF_2 values as obtained from the final f_oF_2 map. (The h_mF_2 values are obtained by exactly the same process used to obtain the f_oF_2 values). See the project algorithm in the next section for details.

SABIM also produces electron density profiles for the South African region, but was not used in the generation of electron density profiles for this work, since the model, being a bottomside ionospheric model, does not produce electron density profiles for the topside ionosphere. In addition, significant time would also be required by the computer programme to combine electron densities from the IRI model and SABIM at each of the altitudes involved in the construction of a single profile. It is also very important to clearly point out at this stage that the electron density profiles generated by adapting the IRI model with f_oF_2 and h_mF_2 values from the map are effectively contributions from all 3 sources used in the development of the map since the f_oF_2 and h_mF_2 values come from a combination of data from all 3 sources.

3.2 The Project Algorithm

The software has a Graphical User Interface (GUI) that makes it more user-friendly, and provides the user with better interaction capability. In this section, the user inputs, processes performed by the programme, and the outputs are discussed.

3.2.1 Required User Inputs

The user is expected to enter the year, month, day, and UT hour of the day for which the map is to be generated. By default, the programme sets these fields to the present year, the present month, the present day of the month, and present time of the day respectively. See figure 3-1 below.

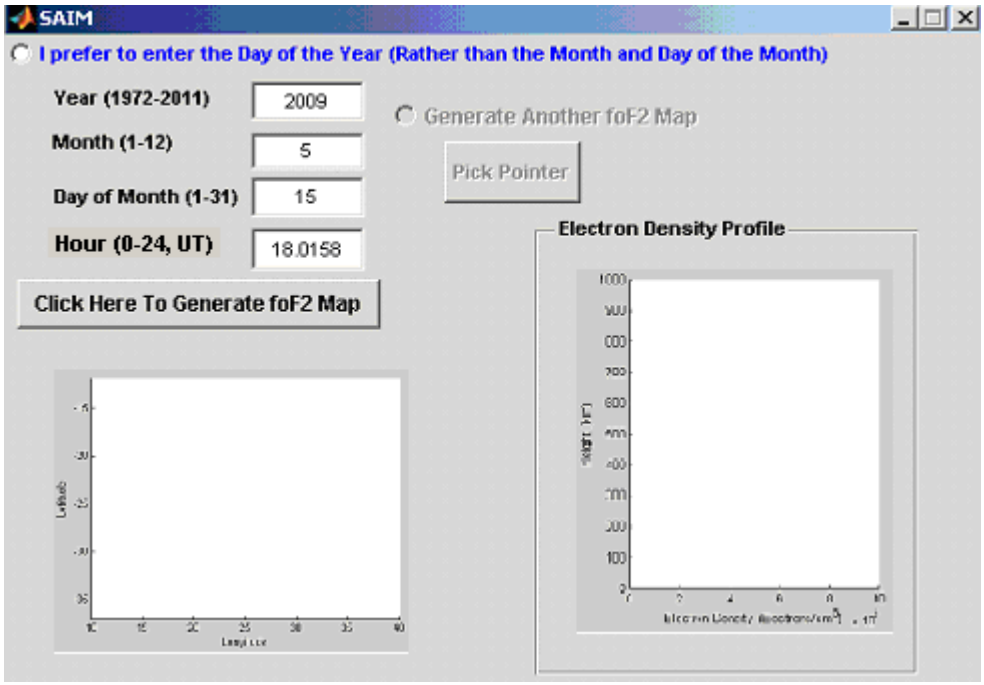

Figure 3-1: The appearance of the GUI when first launched

The software also provides the user with a choice of entering the day of the year, rather than the month and day of the month. To do this, the user has to click on the radio button at the top left of the application, and that portion of the GUI then appears as shown in Figure 3-2.

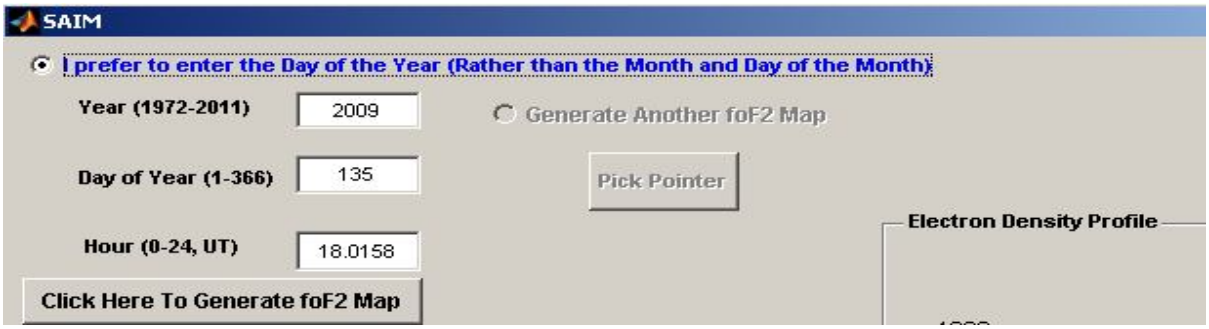

Figure 3-2: Illustrating the use of the radio button at the top left of the application

It is possible for users to edit an input field by entering values of their choice rather than the default values. If a user prefers to enter the month and day of the month, rather than the day of the year, the programme then has to convert them to the appropriate day of the year, for input to the various models.

This version of the software allows the user to generate maps for the periods between 1972 and 2011, the intervals within which the current versions of the IRI and SABIM are both valid. If users enter a year outside the range, they are informed that an invalid year has been entered, and the programme is not executed. The software also alerts the users when they make other invalid inputs like entering 32 for the day of a month.

3.2.2 Generating the f_oF_2 Map

To generate the f_oF_2 map, the user has to click on the command button labeled "Click Here To Generate foF2 Map", and the programme performs the following routine:

1. All inputs are checked to ensure that they are valid. If any of them are not, the user is alerted and the programme execution is terminated. If they are all valid, the programme converts them to the format required by each model, and the programme execution continues.
2. The programme next prepares the input file needed by the SABIM software to generate f_oF_2 values for the entered inputs, and for the locations that fall within longitudes 10º to 40º and latitudes -12º to -37º, a restriction set by the development of the current version of SABIM.
3. It executes the SABIM software and extracts the generated f_oF_2 values from SABIM's output file.

4. Next, the programme prepares the input file needed by the IRI software to generate f_oF_2 values for the entered inputs and for all locations involved, executes the IRI software, and extracts the generated f_oF_2 values from IRI's output file. (The IRI-2007 standard options are used here, see appendix A for illustration).
5. The programme then combines the f_oF_2 values from the SABIM and IRI models to make a two-dimensional map of f_oF_2 values over the South African region; it uses the SABIM f_oF_2 values for places within the triangular region bounded by the 3 ionosonde stations used to develop SABIM, and the IRI f_oF_2 values for places outside the triangular region. It also introduces a smoothing function at the boundary between these regions so that SABIM still contributes outside of the triangular region, but that its contribution fades as the distance to the closest edge of the triangle increases. (The smoothing function is discussed in section 3.4.1).
6. The programme then downloads the latest ionosonde files from the site (which receives them from the ionosonde stations) via file transfer protocol (ftp). If for any reason (the internet is not operational, etc) this site cannot be accessed, the programme continues execution without using the measured ionosonde data. If the site can be accessed, the files are downloaded, and the latest f_oF_2 values from the various ionosonde stations are extracted from their respective ionosonde files. The programme also checks to see if these ionosonde files represent measurements recorded within plus or minus 30 minutes of the time for which the map is required. Only values from within a 60-minute window centered on the map time are used. For each of the ionosonde files to be used, the programme takes the difference between the ionosonde's f_oF_2 measurements and the f_oF_2 value of the ionosonde's location on the map. It then fits a best plane of the differences observed at the various ionosonde locations, and uses this plane to adapt the whole map to the ionosonde's measurements. Section 3.4.2 discusses the plane fit.
7. Finally, the programme produces a graphical colour representation of the ionosphere and displays it as shown in figure 3-3.

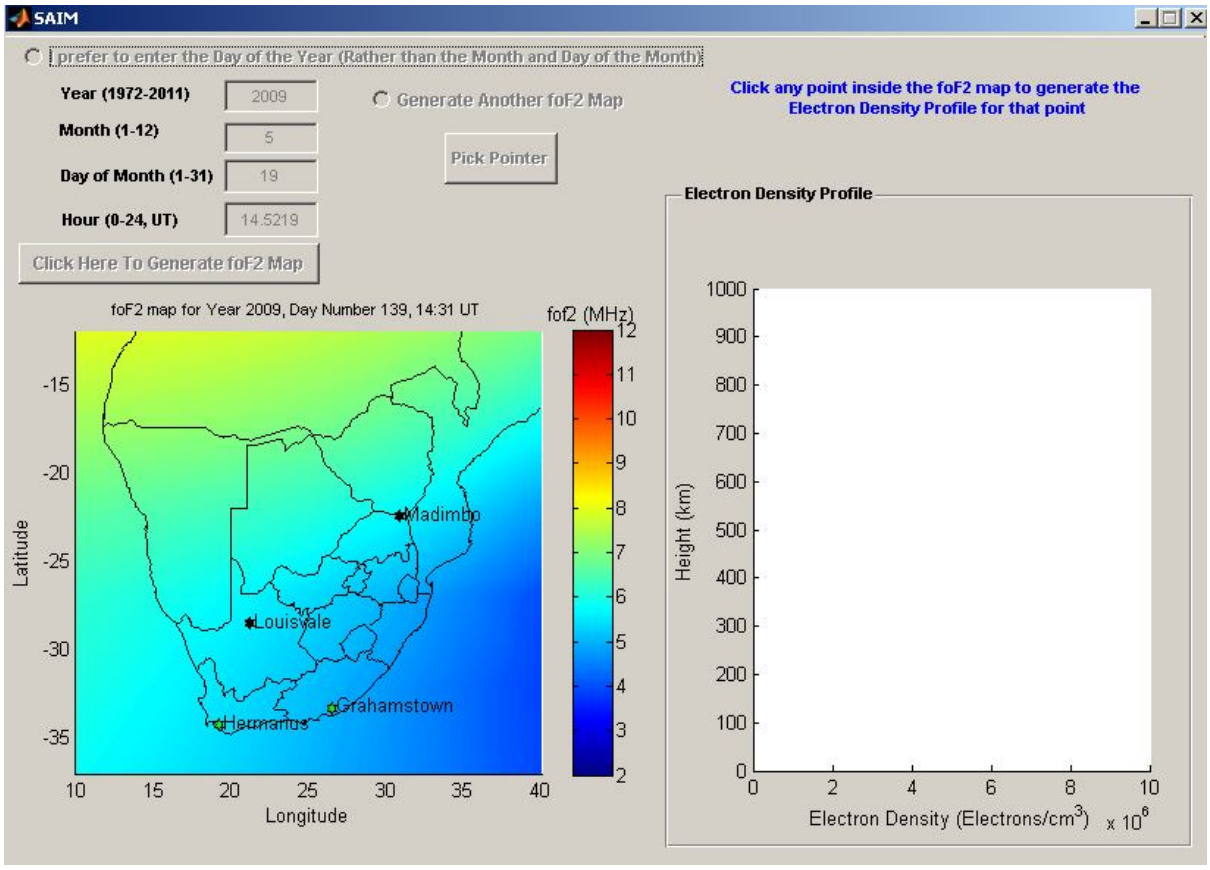

Figure 3-3: The appearance of the GUI after generating the f_oF_2 map

The programme also identifies ionosonde stations from which data was used with green dots, and stations from which data was not used with black dots. In figure 3-3, for instance, data from the Hermanus and Grahamstown ionosondes were used, while those from Louisvale and Madimbo were not used. Data from specific ionosondes may not be used for a variety of reasons including, but not limited to, ionosonde faults or communication delays.

3.2.3 Generating the Electron Density Profile

To generate the electron density profile, the user has to click inside the generated f_oF_2 map at the location for which the electron density profile is to be generated. The programme then performs the following routine.

1. If the user clicks anywhere outside of the f_oF_2 map, the programme does not respond, however inside the f_oF_2 map, the f_oF_2 and h_mF_2 values as well as the longitude and latitude values of the location that the user is interested in are extracted. These values

are then used together with the previous user inputs, as inputs for generating the electron density profile from the IRI model.

2. The programme next prepares the input file as needed by the IRI software to generate the electron density profile for the given inputs. The IRI software is executed and the programme extracts the generated electron density profile data from IRI's output file. (The IRI-2007 standard options are used here, except that f_oF_2 and h_mF_2 values are supplied to the model instead; the IRI model is therefore adapted for the South African f_oF_2 map when generating the electron density profile).
3. Lastly, the programme produces a graphical representation of the electron density profile as illustrated in figure 3-4.

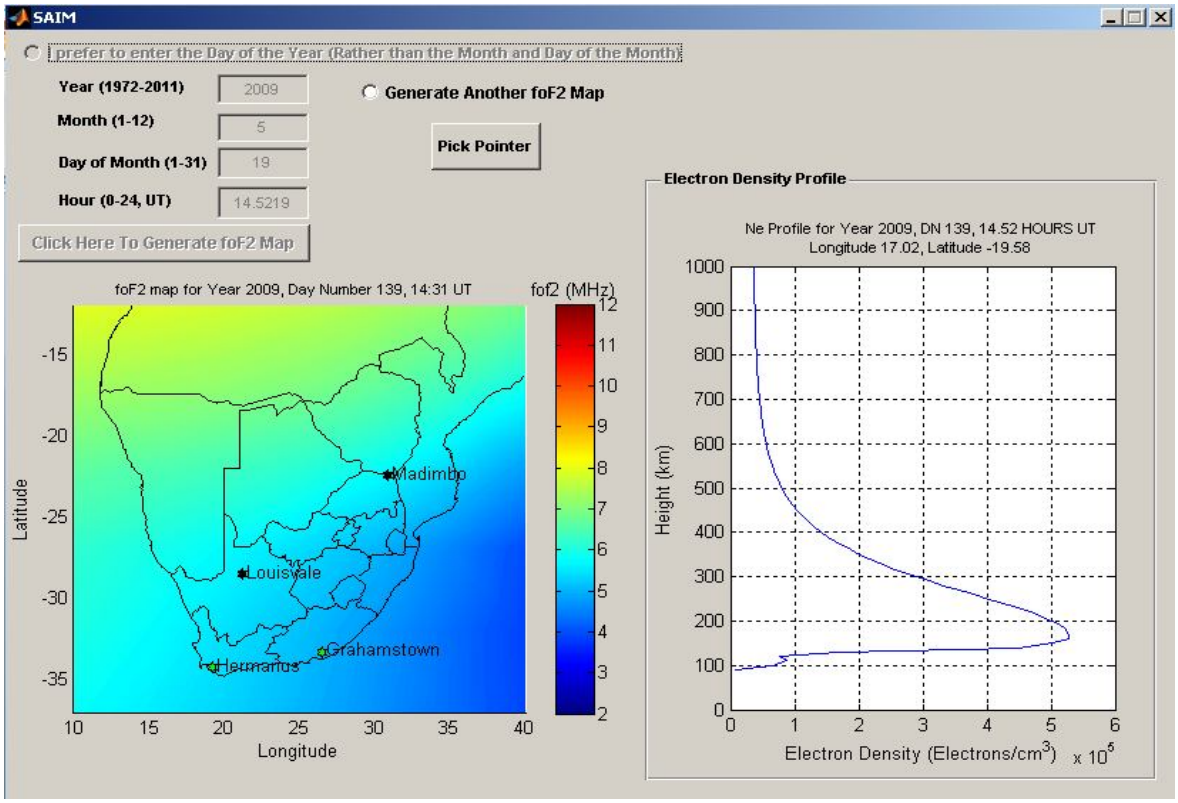

Figure 3-4: The appearance of the GUI after generating an electron density profile

The user, at this stage, can either

i) generate another electron density profile from the current f_oF_2 map using the command button labeled 'Pick Pointer', or

ii) generate a brand new f_oF_2 map for a different set of inputs using the radio button labeled 'Generate Another foF2 map'.

The procedure may be repeated as many times as required.

Prior to finally deciding on a suitable procedure for developing the map (as discussed before), various other options were investigated. One such option, that seemed very viable, is discussed in the next section with reasons why this option was eventually not used in the development of this map.

3.3 Initial Attempts

Initially, the idea was to incorporate the ionosonde data into the f_oF_2 map by using this data only at the ionosonde locations, and then smoothing out into the models. The difficulty with this was that whenever there were significant differences between the ionosonde's observed f_oF_2 values and the models' f_oF_2 values, the generated map showed seemingly special activities (peaks or minimums) at the ionosonde locations. Figure 3-5 illustrates one of these cases.

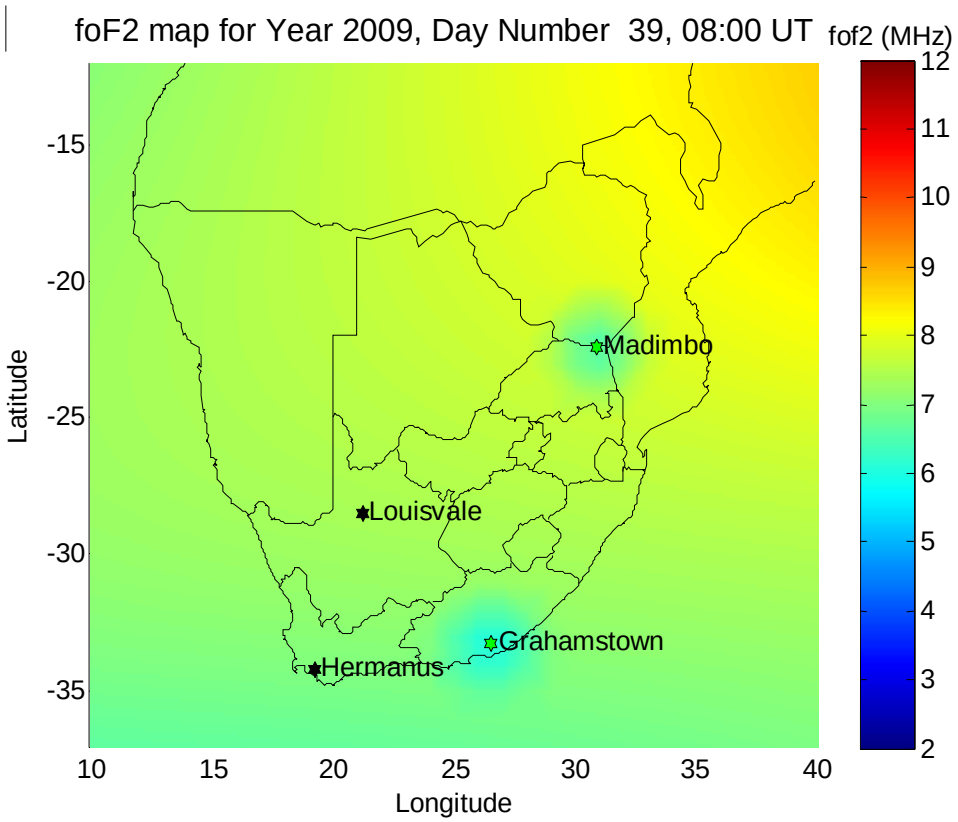

Figure 3-5: An illustration of the seemingly special activities at Madimbo and Grahamstown as a result of the differences between the ionosonde and model values

Figure 3-5 shows lower values of f_oF_2 for Madimbo and Grahamstown than for surrounding places. That outcome is just the result of the differences between the observed ionosonde data and model data, and on a general appearance does not convey the right information about the South African ionosphere. Smoothing the boundaries did not solve the problem as there was always an indication that something different was happening at the ionosonde locations unless the differences were not significant.

An approach that was used to solve the problem was to incorporate the ionosonde measurements (which represent the true state of the ionosphere) in such a way as to affect, not just the ionosonde locations but the whole of the map. A plane fit, in response to the varying degree of the differences between the ionosonde and model values at the ionosonde locations, was used to solve the problem. That plane was used to adapt the whole map to the true ionosonde measurements. Figure 3-6 illustrates what happens when the plane of differences is used for the same condition as in figure 3-5 above.

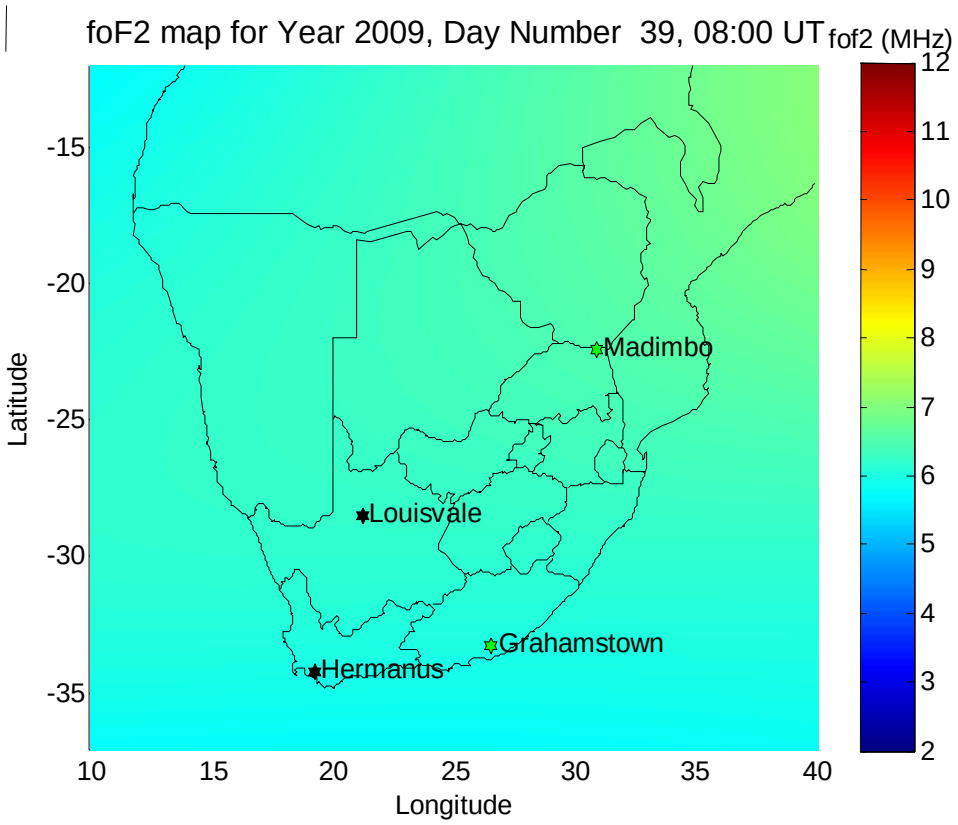

Figure 3-6: Using the plane of differences between the ionosonde and model values to adapt the whole map to measured values

3.4 Mathematical Techniques Used

3.4.1 The Smoothing Function

As explained earlier, to generate the f_oF_2 map, the programme used SABIM inside the triangular region bounded by the 3 ionosonde stations used to develop the model, and the IRI model outside of that region. To ensure a smooth transition at their common boundary, the smoothing function illustrated in equation (3-1) was used. For any given point outside the triangular region, the resulting f_oF_2 value is given by

$$f = f_s \cos^2\theta + f_i \sin^2\theta \qquad (3\text{-}1)$$

where f_s is SABIM's f_oF_2 value for that point, f_i is IRI's f_oF_2 value for the point, and θ is a measure of the point's distance from the closest edge of the triangle. The angle θ was arbitrarily defined to have a value of 0º anywhere on the triangular edge, and 90º at a distance of 10 longitudinal degrees (≈ 1117 km) from the closest triangular edge. For places within 1117 km from the closest triangular edge, the expression θ=90d/1117, was used, where d is the point's distance (in km) from the closest triangular edge. And for places further than 1117 km from the closest triangular edge, the value of θ was defined to remain at 90º so that at those places, SABIM's contribution is zero and the IRI model contribution makes up 100% of the value. In essence, IRI's contribution is zero for points on the triangular edge, increases with distance from the triangle, and is 100% at a distance of 1117 km and beyond from the closest triangular edge.

3.4.2 The Plane Fit

As discussed earlier, the programme adapts the f_oF_2 map to the true ionosonde measurements by fitting a plane of the differences between the measured ionosonde f_oF_2 values and the corresponding f_oF_2 values from the map.

The number of ionosonde stations from which the required data is available represents the number of points to be used to make the plane fit. Usually, 3 points are needed to fit a well-defined plane, but in this case 4 ionosonde stations are available, and it is not likely that the

needed measurements from all 4 will always be available. Any number of points (from 0 to 4) is possible, and the programme's response depends on the number of points available at the time the map is required.

CASE 1: If data from all 4 stations are available, the programme fits a best plane using the least square method as described below.

The general equation of a plane is

$$Ax + By + Cz + D = 0 \tag{3-2}$$

where A, B, C, and D are constants defining the plane.

The perpendicular distance between a point (x_a, y_a, z_a) and the plane is given by

$$d = \frac{Ax_a + By_a + Cz_a + D}{\sqrt{A^2 + B^2 + C^2}} \tag{3-3}$$

For the four points in consideration here, the sum of the squares of their distances will be

$$S = \sum_{i=1}^{4} \frac{(Ax_i + By_i + Cz_i + D)^2}{A^2 + B^2 + C^2} \tag{3-4}$$

where x_i represents the longitudes of the four points, y_i represents their corresponding latitudes, and the z_i represents the corresponding differences in f_oF_2 values at those points.

The best plane is that plane for which S has the least possible value, that is, where

$$\frac{\partial S}{\partial A} = \frac{\partial S}{\partial B} = \frac{\partial S}{\partial C} = \frac{\partial S}{\partial D} = 0 \tag{3-5}$$

This gives the four equations with four unknowns (A, B, C, and D) needed to define the best plane. The programme solves these equations to get the values of the unknowns.

Shakarji (1998), Sturgul & Aiken (1970), and Rust (1972) provided useful information on the techniques used in the fitting of the best plane.

CASE 2: If data from just 3 stations are available, the programme fits the plane passing through those 3 points.

Given any 3 points in space, say (x_i, y_i, z_i) for i=1 to 3, the equation of the plane through them is given as in equation (3-2)

$$Ax + By + Cz + D = 0 \tag{3-2}$$

where

A = the determinant of $\begin{pmatrix} 1 & y_1 & z_1 \\ 1 & y_2 & z_2 \\ 1 & y_3 & z_3 \end{pmatrix}$,

B = the determinant of $\begin{pmatrix} x_1 & 1 & z_1 \\ x_2 & 1 & z_2 \\ x_3 & 1 & z_3 \end{pmatrix}$,

C = the determinant of $\begin{pmatrix} x_1 & y_1 & 1 \\ x_2 & y_2 & 1 \\ x_3 & y_3 & 1 \end{pmatrix}$, and

D = -(the determinant of $\begin{pmatrix} x_1 & y_1 & z_1 \\ x_2 & y_2 & z_2 \\ x_3 & y_3 & z_3 \end{pmatrix}$).

In this case, x_1, x_2, x_3 represent the longitudes of the three points, y_1, y_2, y_3 represent their corresponding latitudes, and z_1, z_2, z_3 represent the corresponding differences in f_oF_2 values at the three points.

CASE 3: If data from only 2 of the stations are available, the programme looks for a third point such that the plane to be fit slopes in the same way as the line joining the 2 points. Suppose the two points are P(x_1, y_1, z_1) and Q(x_2, y_2, z_2), then the programme looks for a third point R(x_3, y_3, z_3) such that R has the same longitude as one of the 2 points (say P), a line drawn from R perpendicularly meets the line PQ at the other point (say Q), and the z value of R is the same as that of Q (that is $z_3 = z_2$). In essence, the desired plane is to contain the line PQ, and to have the same z value at every point on a given perpendicular bisector of line PQ.

CASE 4: If data is available from only 1 of the ionosonde stations, then the plane to be fit is a plane of constant z values; all the points on the plane have the same z value as that of the 1 point.

CASE 5: If no ionosonde data is available, the programme takes no further action on the map generated from the two models; the resulting map is the map obtained from the combination of just the two models.

Ionospheric maps generated using the programme are used to discuss certain physics of the ionosphere in the next section.

3.5 Results

In this section, spatial and temporal variations in the South African ionosphere, as evident in the results of this project, are illustrated. The ionospheric parameter chosen for this illustration is the f_oF_2 value.

3.5.1 Variations during a Typical Day

Figures 3-7a, 3-7b, 3-7c, and 3-7d illustrate, using the map, how the f_oF_2 values vary over a typical day in South Africa. The figures show f_oF_2 maps of the South African ionosphere, as determined by the map described in this thesis, for 8:00 UT (a South African morning), 12:00 UT (a South African afternoon), 14:00 UT (a South African evening), and 22:00 UT (the South African midnight) respectively for day number 13 of year 2009.

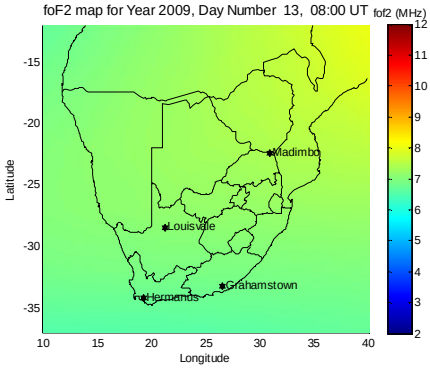

Figure 3-7a: f_oF_2 map of South Africa for a South African morning

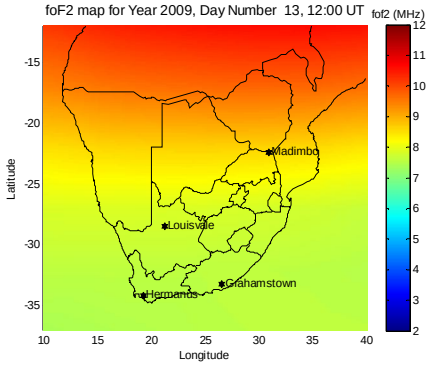

Figure 3-7b: f_oF_2 map of South Africa for a South African afternoon

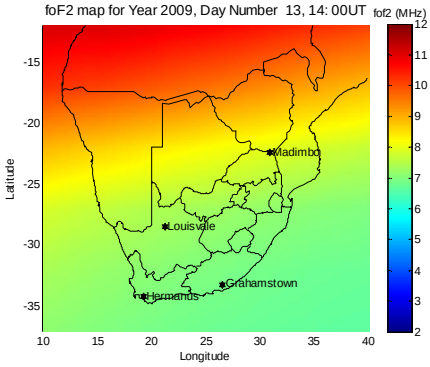

Figure 3-7c: f_oF_2 map of South Africa for a South African evening

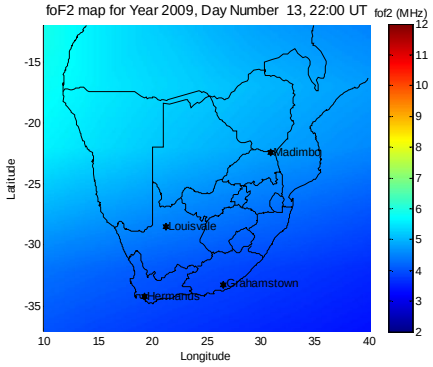

Figure 3-7d: f_oF_2 map of South Africa for a midnight over South Africa

The maps show that the f_oF_2 values are larger in the afternoon than for other parts of the day. This is expected since in the afternoon the sun has fully risen to, or very close to, zenith. The amount of solar radiation reaching the ionosphere during this part of the day is also generally greater than during other parts of the day, giving rise to greater ionospheric electron densities (and hence greater f_oF_2 values). In the early hours of the day (figure 3-7a), the sun is still rising and the f_oF_2 values are therefore relatively lower. During the evening hours, the sun is setting and the f_oF_2 values are therefore gradually decreasing. Nights have the lowest f_oF_2 values due to the absence of solar radiation.

The maps also show that during the early hours of the day (figure 3-7a), the f_oF_2 values are greater at the north-eastern parts, during the afternoon (figure 3-7b), the region of greatest f_oF_2 values shifts towards the north-central parts, and during the evening (figure 3-7c), the

north-western parts have the greatest f_oF_2 values, following the sun's rising from the northeast direction of South Africa and the sun's setting in the northwest direction of the country.

3.5.2 Seasonal Variations

The intensity of solar radiation reaching the ionosphere changes with the seasons of a year. Figures 3-8a, 3-8b, 3-8c, and 3-8d (produced from the ionospheric map of this work) illustrate variations in the South African ionosphere during the 4 seasons of year 2008. The figures are f_oF_2 maps for day numbers 13, 104, 195, and 285 of year 2008, respectively chosen to represent a day in summer, a day in autumn, a day in winter, and a day in spring. The maps are for 10:00 UT (midday local time) for each of the chosen days.

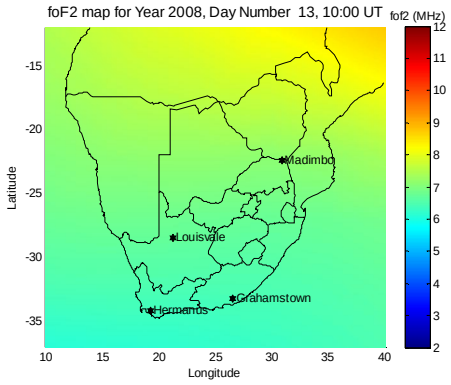

Figure 3-8a: f_oF_2 map of South Africa for a summer day

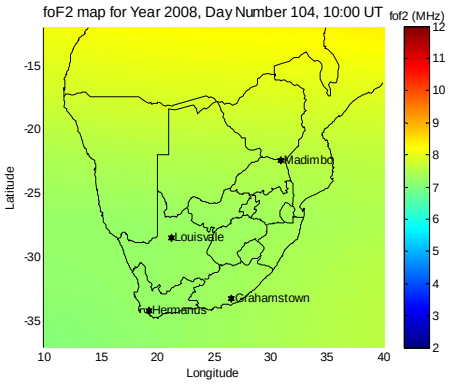

Figure 3-8b: f_oF_2 map of South Africa for an autumn day

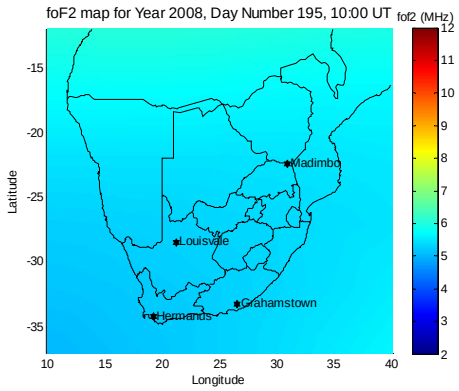

Figure 3-8c: f_oF_2 map of South Africa for a winter day

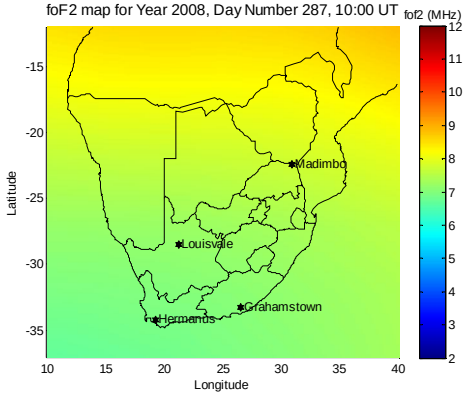

Figure 3-8d: f_oF_2 map of South Africa for a spring day

As expected, the f_oF_2 values are greater for the summer day than for the winter day. The tilt of the Earth's rotational axis relative to the orbital plane coupled with the Earth's revolution round the sun gives rise to these seasons; in summer, a given hemisphere is tilted towards the sun and so experiences greater solar radiation than in winter when the same hemisphere will be tilted away from the sun.

f_oF_2 values at mid latitudes are also greater during the equinoxes (figures 3-8b and 3-8d) than during the solstices (figures 3-8a and 3-8c) due to the mid seasonal anomaly. f_oF_2 data from ionosonde measurements (figure 3-9) also illustrate this.

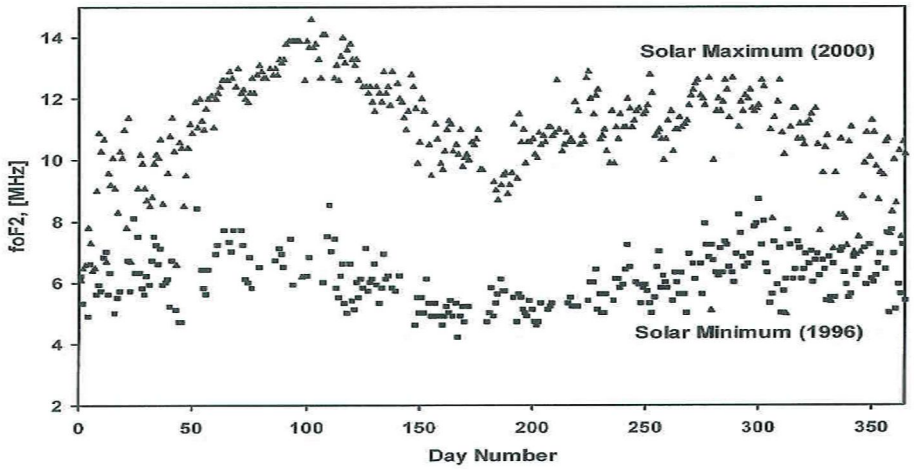

Figure 3-9: The variation in the 10:00 UT (12:00 SAST) f_oF_2 values for a year of solar maximum (2000) and a year of solar minimum (1996) from Gledhill et al (2008, p. 90)

3.5.3 Variations over a Solar Cycle

The ionosphere is also expected to change in response to varying degrees of the solar activity. Figures 3-10a, 3-10b, and 3-10c respectively show the f_oF_2 maps, from this work, for identical periods of year 2000 (a year of solar maximum), year 2003 (a year of moderate solar activity), and year 2006 (a year of minimum solar activity). The maps are for 08:00 UT and day number 50 of each of the chosen years.

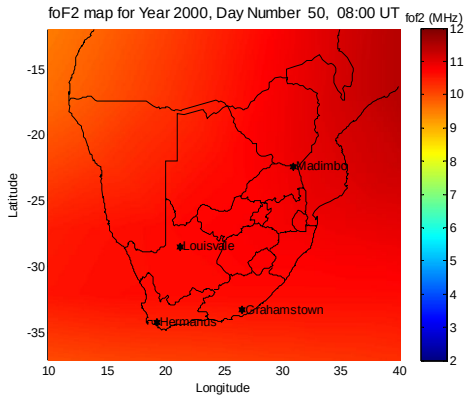

Figure 3-10a: f_oF_2 map of South Africa for a year of maximum solar activity

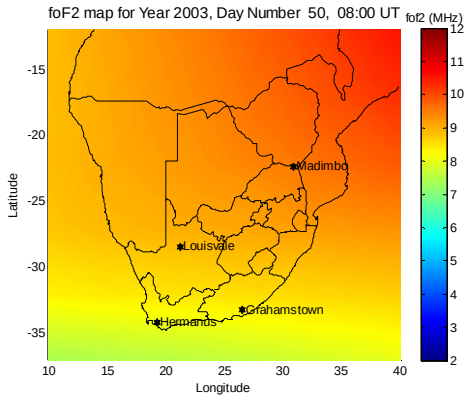

Figure 3-10b: f_oF_2 map of South Africa for a year of moderate solar activity

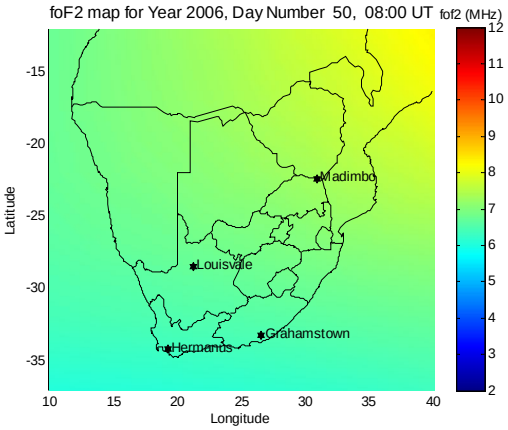

Figure 3-10c: f_oF_2 map of South Africa for a year of minimum solar activity

The ionosphere is also affected by variations in the amount of radiation emitted by the sun. If the solar activity is high, more radiation is emitted by the sun, the ionosphere becomes more ionized because of the greater intensity of solar radiation reaching it, and consequently the f_oF_2 values are greater. The sunspot number (SSN) is a measure of the solar activity. The solar activity (illustrated in figure 3-11) was high in year 2000, moderate in year 2003, and low in year 2006. Figure 3-11 was generated using monthly observations from the Space Physics Interactive Data Resource (SPIDR) website; http://spidr.ngdc.noaa.gov/spidr/.

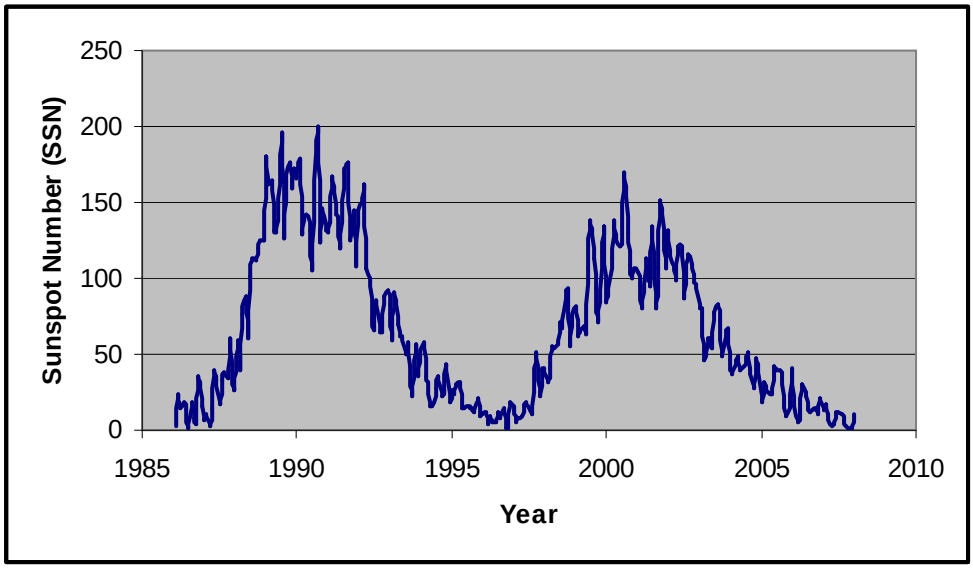

Figure 3-11: A graph illustrating the solar cycle developed by using observed monthly sunspot number values from the SPIDR website

The f_oF_2 maps in figures 3-10a, 3-10b, and 3-10c were generated for exactly the same periods of those 3 different years. The maps show large f_oF_2 values for the year of maximum solar activity, moderate f_oF_2 values for the year of moderate solar activity, and small f_oF_2 values for the year of minimum solar activity.

3.5.4 Latitudinal and Longitudinal Variations

The sun is mostly overhead at locations on, or close to, the equator, and for this reason the sun's radiation is more direct over such places. The overall effect is more ionospheric ionization and hence greater f_oF_2 values for such places. The sun's radiation arrives more obliquely at places farther away from the equator and so there is a gradual degradation in the degree of ionospheric photo-ionization from the equatorial regions to the polar regions.

Longitudinal variations are related to local-time variations. For a given locality, the intensity of solar radiation increases as the sun rises, peaks at about local midday, and decreases as the sun sets.

The maps from this work generally reveal these trends (see figures 3-7a, 3-7b, 3-7c, and 3-7d above) and agree with the fact that the sun's energy is a chief contributor to the ionization of the ionosphere.

Movies were produced based on this work to illustrate the group of variations described in this section. The movies show, graphically and dynamically, the spatial and temporal variations in the f_oF_2 values over the South African region.

The map developed from this work has been tested with a ray-tracing programme and with TEC derived from GPS measurements. The results are discussed in the next chapter.

Chapter 4

Validating the Ionospheric Map

This chapter discusses the project validation, the resources used for the validation and the way in which they have been used to demonstrate the validity of the model.

4.1 Resources Used for Validating the Ionospheric Map

4.1.1 Analytical Ray Tracing

Ray-tracing programmes provide radio communication and radar systems with knowledge of the exact ray path of radio waves as they travel through the ionosphere. The ionospheric map developed in this thesis will be used in conjunction with ray-tracing techniques to locate unknown transmissions, and so it is necessary to demonstrate its usefulness for this purpose.
The ray tracing was carried out using an analytic, path-segmented, quasi-parabolic ray-tracing approach (Norman & Cannon 1997; 1999). The ray-tracing software basically provides a visualization of HF radio traces through the ionosphere for given sets of user inputs.

Users are required to input to the algorithm the locations of the transmitter and receiver stations between which the ray tracing is required. For this project, the ray tracing was performed between Pretoria (25.9ºS, 28.3ºE) and Hermanus (34.3ºS, 19.2ºS). Further required inputs are the date, the time (in UT), and the transmitter frequency (in MHz). It is possible to specify the ionospheric electron density distribution within the ray-tracing algorithm, using either a parameterized ionospheric model (PIM) or a user-specified ionosphere. Either possibility requires the specification of a three-dimensional electron density grid of

longitudes, latitudes, and altitudes to show the electron density values for all points on the grid. To achieve this, the ray-tracing algorithm requires users to enter the following parameters to define the range and resolution of the three-dimensional electron density grid.

i. a minimum height, a maximum height, and a height resolution (in kilometers),
ii. a starting longitude, stopping longitude, and a longitude resolution (in degrees), and
iii. a starting latitude, stopping latitude, and a latitude resolution (in degrees).

For a user-defined ionosphere, the electron density distribution at the grid points must also be specified. Since the requirement here is to validate a new ionospheric map, the user-defined ionosphere option was implemented within the ray-tracing algorithm.

4.1.2 TEC Derived From GPS Data

TEC is the total number of electrons between 2 points in the ionosphere in an imaginary cylinder with a cross-sectional area of 1 m^2. TEC is measured in electrons/m^2, where 10^{16} electrons/m^2 = 1 TEC unit (TECU).

Due to the ionosphere's dispersive nature, radio signals propagating through the ionosphere experience group delays and phase advances (Opperman et al. 2007). Hofmann-Wellenhof et al. (2001, pp. 101-102) showed that the group delays and phase advances are related to the TEC along the signal path by equations (4-1) and (4-2) respectively.

Group delay, $$\Delta_{gr}^{Iono} = \frac{40.3}{f^2} TEC \quad (4\text{-}1)$$

Phase advance, $$\Delta_{ph}^{Iono} = -\frac{40.3}{f^2} TEC \quad (4\text{-}2)$$

where f is the radio frequency.

If a GPS satellite is directly above a receiver, then the TEC derived from such a GPS system is a vertical TEC, otherwise a slant TEC is derived. As GPS satellites are rarely directly above receivers, most of the TEC values derived from the GPS are slant TEC values. Opperman et al. (2007) illustrate the derivation of slant TEC values, and subsequently vertical TEC values, from South African GPS data. The technique they described was used to

derive the vertical GPS-TEC values used in this work. Since these values were only used to validate the map developed in this thesis, and are not part of the map, the details have not been reproduced here.

4.2 Ray Tracing

The three-dimensional electron density grid used in this work covers the longitudes from 10ºE to 40ºE in steps of 2º, latitudes from 13ºS to 37ºS in steps of 2º, and altitudes of 90 km to 900 km in steps of 10 km. The ray tracing was accomplished for two sets of user-defined ionosphere as follows:

i. an ionosphere for which the electron densities at the centre of each grid point were obtained purely from the IRI model using the IRI standard options; this will be referred to as the IRI ionosphere in this work.

ii. an ionosphere for which the electron densities at the centre of each grid point were obtained by using the f_oF_2 and h_mF_2 values from this work to adapt the IRI model; this will be referred to as the MAP ionosphere in this work.

The ray tracing was performed between Pretoria (25.9ºS, 28.3ºE) and Hermanus (34.3ºS, 19.2ºS) with Pretoria as the transmitter station and Hermanus as the receiver station. Pretoria and Hermanus were chosen because of the known HF radio transmission link that exists between the two; transmission by ZS6DN (the international beacon station at Pretoria), and reception by ZS1HMO (the beacon receiver station at the Hermanus Magnetic Observatory, Hermanus). A transmission frequency of 14.000 MHz was used since the ZS6DN beacon transmits at that frequency.

All possible elevation angles and all hours of day numbers 15, 106, 196, and 289 of year 2000 (a year of high solar activity), and year 2006 (a year of low solar activity) were considered. Day numbers 15, 106, 196, and 289 were chosen to respectively represent days in the seasons of summer, autumn, winter, and spring.

The outputs from the ray-tracing software were

i. the hours for which there were rays that arrived within a 30 km radius of the receiver,
ii. the corresponding elevation angles, and
iii. the ground ranges for those transmissions.

The distances between the Hermanus receiver station and where the rays impact the ground were obtained by taking the absolute differences between the ground ranges and the ground distance from Pretoria to Hermanus. The actual ground distance from Pretoria to Hermanus is given as 1295 km. As shown in figure 4-1, if the ground range = R, and the ground distance between Pretoria and Hermanus = D, then the distance between the Hermanus receiver and where the rays impact the ground is d = absolute value of (D – R).

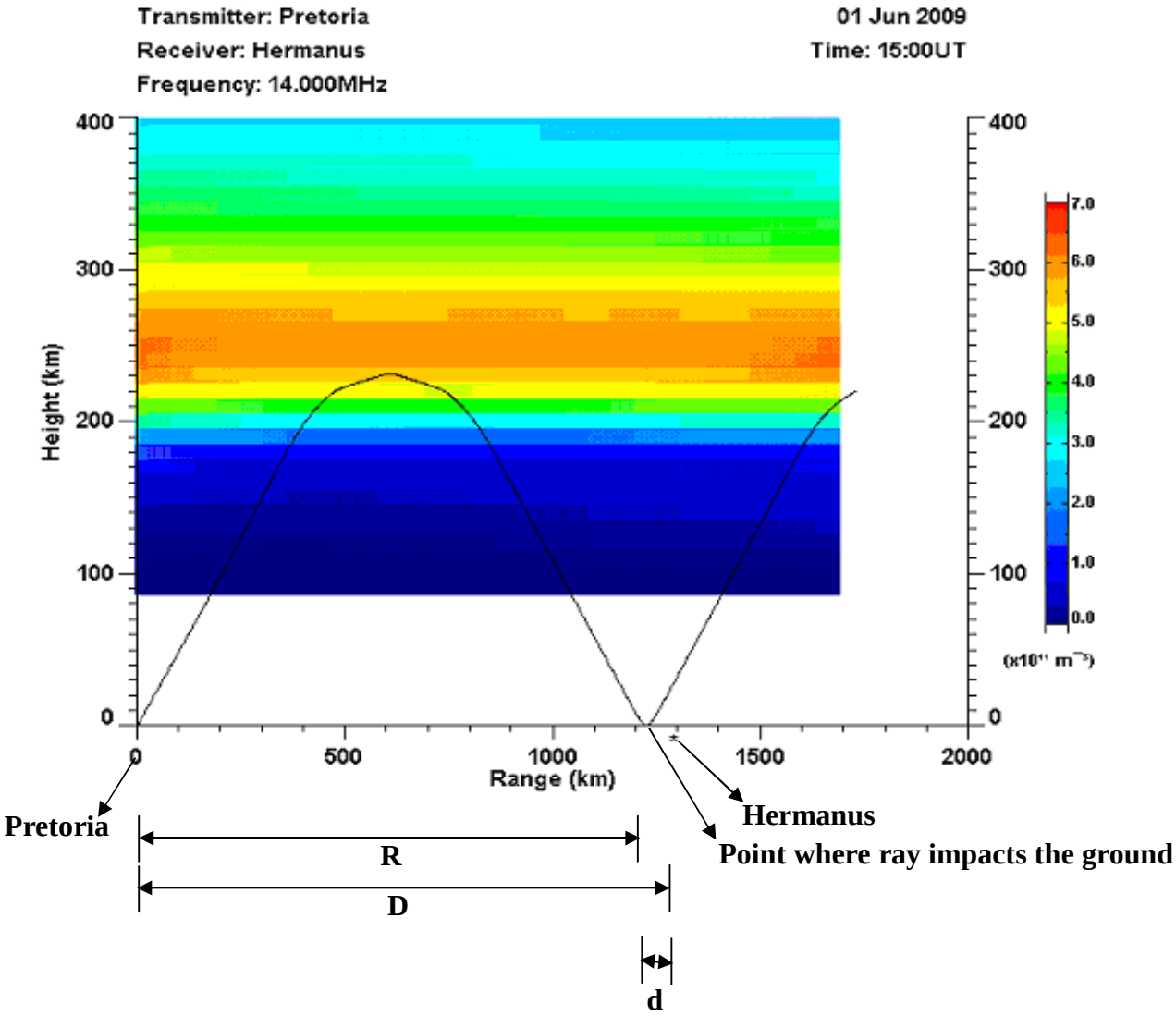

Figure 4-1: An illustration of the procedure used in ray tracing

Tables B-1 to B-8 in appendix B summarize the results of the ray tracing. Hours and elevation angles for which no rays arrived within a 30 km radius of the receiver were not shown. The empty cells in the tables represent hours and elevation angles for which using one of the MAP or IRI ionospheres produced rays arriving within a 30 km radius of the receiver but using the other did not.

Table 4-1 contains information for the number of times that there were rays arriving within a 30 km radius of the Hermanus receiver, using both maps.

Table 4-1: The ray-tracing results for the number of times that there were rays arriving within a 30 km radius of the Hermanus receiver, using both maps

Year	Day of the Year	Hour of the Day (UT)	Elevation Angles of Rays Arriving within 30 km of the Hermanus Receiver (degrees)	Distance from Hermanus Receiver (km)	
				Using the IRI Ionosphere	Using the MAP Ionosphere
2000	15	6	7.50	22.86	20.14
			25.00	4.70	3.14
	106	8	40.00	22.79	8.07
		11	7.50	8.04	8.43
			20.00	25.95	3.62
			60.00	28.08	28.18
		12	45.00	25.37	20.85
		13	45.00	22.54	14.72
	196	8	7.50	22.64	20.23
		9	7.50	7.55	7.40
		10	7.50	7.33	8.52
	289	6	7.50	26.07	24.95
		11	10.31	7.56	2.38
		12	7.50	18.72	17.64

The ray-tracing results (including those illustrated in appendix B) show that

1. Most of the rays that arrived within a 30 km radius of Hermanus from Pretoria were transmitted at elevation angles of between 7.5 and 40.0 degrees.

2. The percentage of rays arriving close to Hermanus from Pretoria was larger when using the MAP ionosphere than when using the IRI ionosphere. For the number of times that there were rays arriving within 30 km radius of the Hermanus receiver, using both maps, the rays arrived closer to the Hermanus station using the MAP ionosphere than they did using the IRI ionosphere. This happened for 78.6% of the cases.

In conclusion the MAP ionosphere appears to offer a better transmission link between Pretoria and Hermanus than the IRI ionosphere. It should be noted that this was a very narrow study intended to demonstrate a practical use of the ionospheric map developed in this work. A more accurate study could be accomplished with access to signal strength data from an automatic monitoring station.

4.3 Comparisons with GPS-Derived TEC

This section illustrates the comparison of vertical GPS-derived TEC values with vertical TEC values obtained as follows:

i. Vertical TEC values were derived from the map using the IRI model; the IRI model was supplied with f_oF_2 and h_mF_2 values from the map so as to output the TEC values. For simplicity and quick identification, TEC values derived using this method will be referred to as MAP-TEC in this work.

ii. Vertical TEC values were also obtained from the IRI model using the standard IRI options illustrated in appendix A. For simplicity and quick identification, TEC values derived using this method will be referred to as IRI-TEC in this work

Vertical TEC values derived from GPS data will be referred to as GPS-TEC.

To obtain the MAP-TEC and the IRI-TEC, the upper integration limit of the IRI model was set to 20200 km (the altitude of the GPS satellites).

GPS data from the following three dual-frequency GPS receiver stations within South Africa were used. The stations were chosen to cover certain regions of interest.

i. The Bloemfontein station (26.3ºE, 29.1ºS) was chosen to be representative of places inside the quadrilateral region bounded by the 4 ionosonde stations in the South African ionosonde network. Bloemfontein is in the central part of the country.

ii. The Calvinia station (19.8ºE, 31.5ºS) was chosen to be representative of places outside the quadrilateral region bounded by the 4 ionosonde stations in the South African ionosonde network. Calvinia lies in the southwestern part of the country.

iii. The Pietersburg station (29.5ºE, 23.9ºS) was chosen to be representative of places close to the ionosonde stations. Pietersburg is close to Madimbo, in the northeastern part of the country.

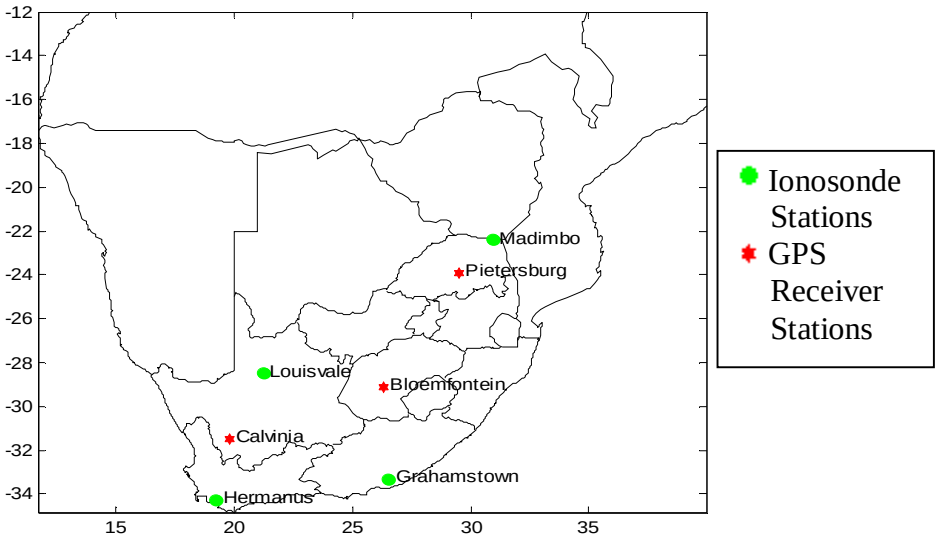

Figure 4-2: Location of the GPS receiver stations used in relation to the ionosonde stations

Available GPS-TEC values for 10:00 UT of each day were used. IRI-TEC values and MAP-TEC values corresponding to these times were obtained. Figures 4-3, 4-4, and 4-5 illustrate how the IRI-TEC and MAP-TEC values compare with the GPS-TEC values at the three selected GPS receiver stations.

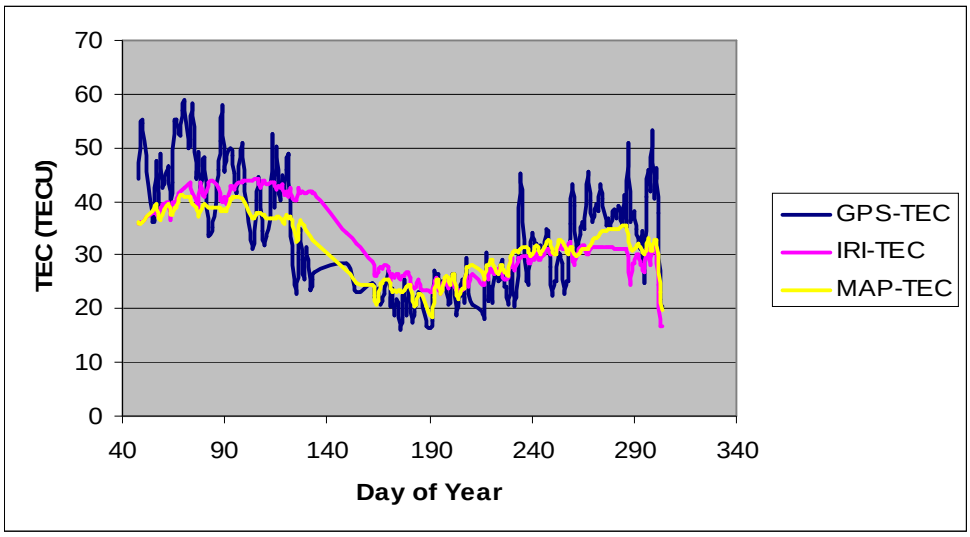

Figure 4-3: Comparison of the 10:00 UT TEC values at Bloemfontein for year 2003

For figures 4-3, 4-4, and 4-5 sample sizes of 201, 189, and 135 data points respectively were available. The correlations related to these examples are given in table 4-2.

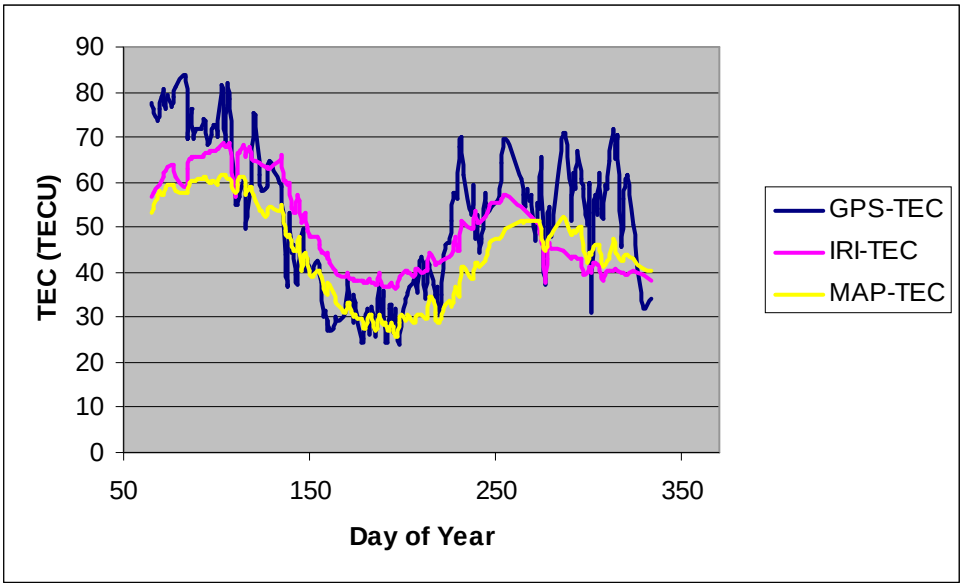

Figure 4-4: Comparison of the 10:00 UT TEC values at Calvinia for year 2002

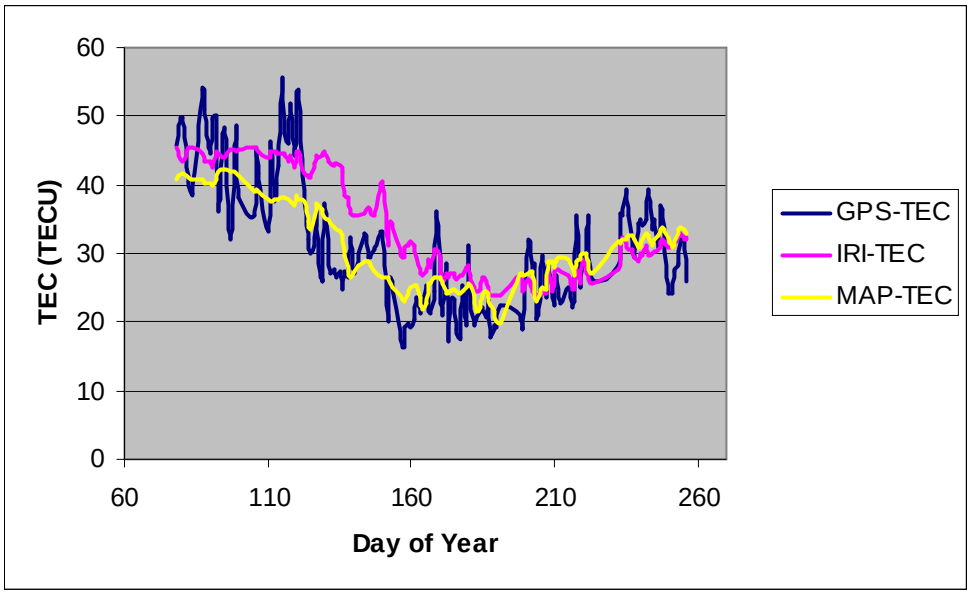

Figure 4-5: Comparison of the 10:00 UT TEC values at Pietersburg for year 2003

Table 4-2: Correlation of the IRI-TEC values and the MAP-TEC values with the GPS-TEC values

Station	Correlation Coefficient between GPS-TEC and IRI-TEC	Correlation Coefficient between GPS-TEC and MAP-TEC	Sample Size
Bloemfontein	0.69	0.83	201
Calvinia	0.73	0.85	189
Pietersburg	0.72	0.83	135

Generally, both the IRI-TEC values and the MAP-TEC values correlate well with the GPS-TEC values, but the results show a better correlation between the MAP-TEC and the GPS-TEC than the correlation between the IRI-TEC and the GPS-TEC. This further validates the idea of using the f_oF_2 map from this work to adapt the IRI model for the South African Region. Future work that could be carried on from this project is discussed in chapter 5.

Chapter 5

Conclusion and Future Work

5.1 Discussion and Conclusion

In order to fully utilize the South African ionosphere for the purpose of HF communications, an ionospheric map is required. However, aviation industries, and most of the industries that make use of Earth-Space systems, also require ionospheric maps to adequately correct for the effects the ionosphere has on their systems. High frequency radio communication industries use such maps in conjunction with ray-tracing algorithms for direction finding and prediction of propagation conditions. The idea behind this work is to produce the best possible representation of the South African ionosphere given the available resources. The IRI model, SABIM, and ionosondes in the South African Ionosonde Network were utilized; the sources were incorporated into the map in such a manner as to provide an accurate description of the South African ionosphere. The map has been tested and demonstrated for practical application, since a significant aim of this project was to make the map as applicable as possible.

A potential user of the map is GrinTek Ewation (GEW) who is currently evaluating it for their purposes. In response to their wishes for the map, the current version of the map has been expanded to also generate h_mF_2 values using exactly the same techniques that were used for generating f_oF_2 values for the map. Graphical representations of the h_mF_2 values will be made in subsequent versions of the software.

A major limitation of the map is that it is spatially constrained to the South African region, a great concern for users who will be interested in using the map beyond these boundaries. The possibility of expanding the map to include other African countries, and the portability of the map to other countries of the world, such as India, which has similar requirements to South Africa, were discussed with Grintek Ewation and has been proposed for future work. It is hoped that the map will subsequently be developed to suit the needs of various users.

5.2 Future Work

In this section, improvements to the performance and scope of the map are suggested.

The map accuracy can be improved using signal strength data from known HF radio transmission links like the one between Pretoria and Hermanus. Signal strength data obtained from the receiver station could be used as an indication of how close to the receiver the signals from the transmitter are arriving. Using ray tracing, the map is then harmonized to match the observed transmission conditions.

Other ionospheric parameters like TEC can also be incorporated into the map. Potential sources of data include

i. TEC derived from GPS data (see Opperman et al (2007)),
ii. TEC predicted from NNs (see Habarulema et al (2009)), and
iii. TEC predicted from the IRI model (with the IRI model supplied with f_oF_2 and h_mF_2 values from this map)

The ideas used in this work, can also be extended to cover other parts of the African continent. A major deterrent to achieving this is the paucity of ionospheric information available for the continent, especially from ionosondes. However, given the increased availability of GPS receivers, GPS data may be used in conjunction with the available models. Since ionosondes are the best sources of bottomside ionospheric information, their installation across different parts of the continent would greatly improve the accuracy of ionospheric maps for the continent.

In conclusion, since the accuracy of the map greatly depends on that of the models used, and since both models are regularly updated, a significant way to improving the accuracy of the

map would be to regularly update it in line with the models, ensuring that the latest version of each model is incorporated into the map. The plan is to update the map regularly so as to maintain desirable accuracies. Such a map of the ionosphere should find fruitful application in HF radio communication, aviation, space weather, ionospheric climatology, and error corrections in GPS and satellite links.

Appendix A

IRI Standard Options

Table A-1: The IRI Standard Options

Available Options		IRI Standard Options
True	**False**	
Ne computed	Ne not computed	True
Te, Ti computed	Te, Ti not computed	True
Ne & Ni computed	Ni not computed	True
B0 - Table option used	B0 - Gulyaeva (1987) used	True
f_oF_2 – CCIR used	f_oF_2 – URSI used	False
Ni - DS-78 & DY-85 used	Ni - DS-95 & TTS-03 used	False
Ne – Topside: f10.7<188	Ne – Topside: f10.7 unlimited	True
f_oF_2 from model	f_oF_2 or N_mF_2 - user input	True
h_mF_2 from model	h_mF_2 or M3000F2 - user input	True
Te – Standard	Te - Using Te/Ne correlation	True
Ne - Standard Profile	Ne - Lay-function formalism	True
Print messages to screen	No messages	True
f_oF_1 from model	f_oF_1 or N_mF_1 - user input	True
h_mF_1 from model	h_mF_1 - user input (only Lay version)	True
f_oE from model	f_oE or N_mE – user input	True
h_mE from model	h_mE - user input	True
Rz12 from file	Rz12 - user input	True
IGRF dip, magbr, modip	Old FIELDG using POGO68/10 for 1973	True
F1 probability model	Critical solar zenith angle (old)	True
standard F_1	Standard F_1 plus L condition	True
Ion drift computed	Ion drift not computed	False

Ion densities in percentage	Ion densities in m^{-3}	True
Te_topside (Aeros,ISIS)	Te_topside (Intercosmos)	False
D-region: IRI-95	Special: 3 D-region models	True
F107D from AP.DAT	F107D - user input	True
f_oF_2 storm model	No storm updating	True
IG12 from file	IG12 - user input	True
Spread-F probability computed	Spread-F probability not computed	False
IRI01-topside	New options for topside	False
IRI01-topside corrected	NeQuick topside model	False

Appendix B

Ray-tracing Results

Table B-1: Ray-tracing results for day number 15 of year 2000

Hour (UT)	Elevation Angles of Rays Arriving within 30 km of the Hermanus Receiver (degrees)	Distance from Hermanus Receiver (km)	
		Using the IRI Ionosphere	Using the MAP Ionosphere
5	26.25		18.98
	30.00	23.07	
6	7.50	22.86	20.14
	25.00	4.70	3.14
	30.00		23.99
7	10.63		15.58
	25.00	21.76	
	35.00		25.61
8	30.00		0.75
9	30.00		0.72
	42.50	0.44	
10	28.22		1.02
12	10.00	28.68	
13	25.00	28.81	
14	30.00		28.67
	35.00		27.40
	30.00		28.01
15	30.00		3.39
16	30.00		0.16

Table B-2: Ray-tracing results for day number 106 of year 2000

Hour (UT)	Elevation Angles of Rays Arriving within 30 km of the Hermanus Receiver (degrees)	Distance from Hermanus Receiver (km)	
		Using the IRI Ionosphere	Using the MAP Ionosphere
4	20.00	8.03	
6	18.63		22.63
	60.04	10.38	
7	7.50		15.63
8	10.00	14.37	
	15.98	15.47	
	40.00	22.79	8.07
9	16.72		26.16
	18.54	26.97	
	40.00		5.47
	60.00		13.52
10	19.01		20.47
	19.49	12.97	
	40.00		1.73
	60.00	18.99	
11	7.50	8.04	8.43
	19.70	12.10	
	20.00	25.95	3.62
	20.14		9.38
	60.00	28.08	28.18
12	19.23	12.80	
	20.00		0.91
	20.04		3.06
	45.00	25.37	20.85
	60.00		5.77
13	18.48	13.37	
	19.27		1.08

	45.00	22.54	14.72
	65.00		21.07
14	45.00		14.91
15	18.95		16.43
	20.00	10.62	
16	20.00		30.00
	20.81		0.05
	25.00	9.47	
17	30.00		27.59

Table B-3: Ray-tracing results for day number 196 of year 2000

Hour (UT)	Elevation Angles of Rays Arriving within 30 km of the Hermanus Receiver (degrees)	Distance from Hermanus Receiver (km)	
		Using the IRI Ionosphere	Using the MAP Ionosphere
5	17.25	11.31	
6	14.20	10.53	
7	14.69	12.08	
8	7.50	22.64	20.23
	16.81	24.45	
9	7.50	7.55	7.40
	40.00	13.43	
10	7.50	7.33	8.52
	19.04	21.64	
	45.00		6.13
11	18.91	21.70	
	19.73		21.66
	20.00		21.30
	45.00		3.02
	47.50		22.34
12	18.18	22.46	
	19.46		6.37
	45.00		16.48
	47.50		7.43
13	17.39	18.29	
	19.06		21.31
	45.00	29.34	
	47.50	28.21	
14	16.86	27.10	
	18.53		14.10
15	18.68		17.57
	19.03	14.96	

Table B-4: Ray-tracing results for day number 289 of year 2000

Hour (UT)	Elevation Angles of Rays Arriving within 30 km of the Hermanus Receiver (degrees)	Distance from Hermanus Receiver (km)	
		Using the IRI Ionosphere	Using the MAP Ionosphere
5	20.00	21.26	
	19.72	7.81	
6	7.50	26.07	24.95
	20.86	12.50	
7	22.40	19.99	
8	23.42	18.01	
	25.73		3.69
9	25.00	22.24	
	24.70	6.06	
10	23.90	14.42	
11	10.31	7.56	2.38
	23.47	15.44	
12	7.50	18.72	17.64
	22.33	0.57	
	25.00		22.35
13	20.00	12.00	
	19.89	7.28	
16	21.22		3.84
17	32.50	10.54	
	25.00	1.56	

Table B-5: Ray-tracing results for day number 15 of year 2006

Hour (UT)	Elevation Angles of Rays Arriving within 30 km of the Hermanus Receiver (degrees)	Distance from Hermanus Receiver (km)	
		Using the IRI Ionosphere	Using the MAP Ionosphere
6	19.06		25.17
8	24.69		7.54
	25.50		20.91
9	24.69		14.45
10	25.47		6.74
12	23.59		20.18
13	24.92		7.46
	25.00		23.59
14	22.50		11.71
16	21.56		11.64
	25.17		25.34

Table B-6: Ray-tracing results for day number 106 of year 2006

Hour (UT)	Elevation Angles of Rays Arriving within 30 km of the Hermanus Receiver (degrees)	Distance from Hermanus Receiver (km)	
		Using the IRI Ionosphere	Using the MAP Ionosphere
6	26.11	0.25	
	18.35	9.47	
7	28.91	12.43	
	17.84	0.92	
8	18.61	7.03	
9	19.89	4.77	
	20.00	9.10	
	22.05		16.01
	28.90	15.07	
	29.69		20.25
10	20.00	7.79	
	20.40	9.60	
	22.95		29.88
	28.49	28.76	
	29.17		27.95
11	19.98	3.05	
	20.00	3.92	
	24.22		29.69
	28.13	4.99	
12	19.80	7.49	
	20.00	11.80	
	23.38		26.05
	26.51	10.79	
13	21.59		5.72
14	22.50		13.85
	25.00		26.76
	25.63		21.99

	26.59		29.68
15	22.65		27.26

Table B-7: Ray-tracing results for day number 196 of year 2006

Hour (UT)	Elevation Angles of Rays Arriving within 30 km of the Hermanus Receiver (degrees)	Distance from Hermanus Receiver (km)	
		Using the IRI Ionosphere	Using the MAP Ionosphere
9	22.50		14.09
10	24.38		22.48
11	25.31		4.31
12	20.63		28.89
	25.31		11.09
13	19.90		14.26
	20.00		18.78
	20.04		20.46
	25.00		22.28

Table B-8: Ray-tracing results for day number 289 of year 2006

Hour (UT)	Elevation Angles of Rays Arriving within 30 km of the Hermanus Receiver (degrees)	Distance from Hermanus Receiver (km)	
		Using the IRI Ionosphere	Using the MAP Ionosphere
10	25.00	25.80	
	26.25	23.54	
11	24.88	4.99	
	25.00	6.73	
	26.25	13.71	
12	24.09	12.98	
	25.00	28.11	
	26.25	16.50	
13	25.00	18.91	
	27.50		12.22
14	20.92		7.66
	22.91		18.77
15	20.60		7.79
	26.88		8.19

References

Adewale, AO, Oyeyemi, EO & Mckinnell, LA 2009, 'Comparisons of Observed Ionospheric F2 Peak Parameters with IRI-2001 Predictions over South Africa', *Journal of Atmospheric and Solar-Terrestrial Physics*, vol. 71, issue 2, pp. 273-284.

Bhuyan, PK & Borah, RR 2007, 'TEC Derived from GPS Network in India and Comparison with the IRI', *Advances in Space Research*, vol. 39, issue 5, pp. 830-840.

Bilitza, D 2001, 'International Reference Ionosphere 2000', *Radio Science*, vol. 36, no. 2, pp. 261-275.

Bilitza, D & Reinisch, BW 2008, 'International Reference Ionosphere 2007: Improvements and New Parameters', *Advances in Space Research*, vol. 42, issue 4, pp. 599–609.

Bilitza, D, Rawer, K, Bossy, L & Gulyaeva, T 1993, 'International Reference Ionosphere, Past, Present, and Future: I. Electron Density', *Advances in Space Research*, vol. 13, no. 3, pp. (3)3-(3)13.

Bonnet, R & Woltjer, L 2008, *Surviving 1,000 Centuries: Can we do it?*, Springer.

Chen, FF 1984, *Introduction to Plasma Physics and Controlled Fusion*, Second Edition, Springer.

Chuo, YJ & Lee, CC 2008, 'Ionospheric Variability at Taiwan Low Latitude Station: Comparison between Observations and IRI-2001 Model', *Advances in Space Research*, vol. 42, issue 4, pp. 673-681.

Davies, K 1990, *Ionospheric Radio*, Institution of Engineering and Technology.

De Medeiros, RT, Souza, JR, Abdu, MA, Batista, IS, Soberal, JHA & Borba, GL 2003, 'Comparisons of IRI Model and Electron Density Data for the Sub-Equatorial Station,

Natal, *Advances in Space Research*, vol. 31, issue 3, pp. 557-561.

Gledhill, JA, Poole, AWV & McKinnell LA 2008, *NASSP Aeronomy Course 2008*, Aeronomy Lecture Note for the National Astrophysics and Space Science Progamme.

Giraud, A & Petit, M 1978, *Ionospheric Techniques and Phenomena*, Springer.

Grintek Ewation 2009, *Company Overview.* Retrieved May 5, 2009, from http://www.gew.co.za/.

Gurney, K 1997, *An Introduction to Neural Networks*. CRC Press.

Habarulema, JB, McKinnell, LA & Opperman, BDL 2009, 'Towards a GPS-Based TEC Prediction Model for Southern Africa with Feed Forward Networks', *Advances in Space Research*, vol. 44, issue 1, pp. 82-92.

Haselgrove, J 1955, 'Ray Theory and a New Method for Ray Tracing', *London Physical Society Report of Conference on the Physics of the Ionosphere*, pp. 355-364.

HMO (Hermanus Magnetic Observatory) 2009, *South African Ionospheric Stations.* Retrieved May 5, 2009, from http://spaceweather.hmo.ac.za/index.php?action=info&topic=IONOSONDE.

Hofmann-Wellenhof, B, Lichtenegger, H & Collins, J 2001, *GPS: Theory and Practice*, Fourth Edition, Springer.

Kohl, H, Ruster, R & Schlegel, K 1996, *Modern Ionospheric Science*, European Geophysical Society, Germany.

Lorentz, HA 1916, *The Theory of Electrons*, Second Edition, Leipzig.

McKinnell, LA 2002, 'A Neural Network Based Ionospheric Model for the Bottomside Electron Density Profile over Grahamstown, South Africa', PhD Thesis, Rhodes University.

McKinnell, LA 2005, *The LAM Model, Version 2.0, A Bottomside Ionospheric Model for the South African Region.* Technical Report for Grintek.

McKinnell, LA 2008a, 'Using Neural Networks to Determine the Optimum Solar Input for the Prediction of Ionospheric Parameters', *Advances in Space Research*, vol. 42, issue 4 pp. 634-638.

McKinnell, LA 2008b, *SABIM Model Version 3.0: A Bottomside Ionospheric Model for the South African Region.* Technical Report for Grintek.

McKinnell, LA 2008c, *An Electron Density Profile Model for the South African Ionosphere*. Retrieved May 5, 2009, from http://cnfrs.institut-telecom.fr/pages/pages_ursi/URSIGA08/papers/G02p2.pdf.

McKinnell, LA 2008d, 'Introducing Hermanus HE13N (34.4°S, 19.2°E): A New Southern Hemisphere Ionosonde Station in South Africa', *INAG Bulletin on the Web*. Retrieved May 5, 2009, from http://www.ips.gov.au/IPSHosted/INAG/web-69/2008/introducing_hermanus.pdf.

McKinnell, LA & Poole, WA 2004, 'Neural Network-Based Ionospheric Modelling over the South African Region', *South African Journal of Science*, vol. 100, pp. 519-523.

McNamara, LF & Wilkinson, PJ 1983, 'Prediction of Total Electron Content using the International Reference Ionosphere', *Journal of Atmospheric and Terrestrial Physics*, vol. 45, issues 2-3, pp. 169-174.

Norman, RJ & Cannon, PS 1997, 'A Two-Dimensional Analytic Ray-Tracing Technique Accommodating Horizontal Gradients', *Radio Science*, vol. 32, no. 2, pp. 387-396.

Norman, RJ & Cannon, PS 1999, 'An Evaluation of a New 2-D Analytic Ionospheric Ray-Tracing Technique – SMART', *Radio Science*, vol. 34, no. 2, pp. 489-499.

Opperman, BDL, Cilliers, PJ, McKinnell, LA & Haggard, R 2007, 'Development of a

Regional GPS-Based Ionospheric TEC Model for South Africa', *Advances in Space Research*, vol. 39, issue 5, pp. 808-815.

Poole, AWV & McKinnell, LA 2000, 'On the Predictability of foF2 using Neural Networks', *Radio Science*, vol. 35, pp. 225-234.

Ratcliffe, AJ 1972, *An Introduction to the Ionosphere and Magnetosphere*, CUP Archive.

Rust, WM 1972, 'Comments on the Best Plane through Data', *Mathematical Geology*, vol. 4, no. 1, pp. 73-75.

Sethi, NK, Dabas, RS & Sharma, K 2008, 'Comparisons between IRI Predictions and Digital Ionosonde Measurements of hmF2 at New Delhi during Low and Moderate Solar Activity', *Journal of Atmospheric and Solar-Terrestrial Physics*, vol. 70, issue 5, pp. 756-763.

Sethi, NK, Dabas, RS & Upadhayaya 2009, 'Midday Bottomside Electron Density Profiles during Moderate Solar Activity and Comparison with IRI-2001', *Advances in Space Research*, vol. 43, issue 6, pp. 973-983.

Shakarji, CM 1998, 'Least-Squares Fitting Algorithms of the NIST Algorithm Testing System', *Journal of Research of the National Institute of Standards and Technology*, vol. 103, No. 6, pp. 633-641.

Soicher, H, Gorman, F, Tsedilina, EE & Weitsman, OV 1995, 'Comparison of the IRI-90 with Measured Ionospheric Parameters at Midlatitudes', *Advances in Space Research*, vol. 16, issue 1, pp. 129-132.

SPIDR (Space Physics Interactive Data Resource), http://spidr.ngdc.noaa.gov/spidr/.

Sturgul, JR & Aiken, C 1970, 'The Best Plane through Data', *Mathematical Geology*, vol. 2, no. 3, pp. 325-331.

UMLCAR (University of Massachusetts Lowell's Center for Atmospheric Research),

Background to Ionospheric Sounding. Retrieved May 5, 2009, from http://ulcar.uml.edu/digisonde_dps.html.